Document made available under the Patent Cooperation Treaty (PCT)

International application number: PCT/US04/040872

International filing date: 06 December 2004 (06.12.2004)

Document type: Certified copy of priority document

Document details: Country/Office: US
Number: 60/527,209
Filing date: 04 December 2003 (04.12.2003)

Date of receipt at the International Bureau: 02 September 2005 (02.09.2005)

Remark: Priority document submitted or transmitted to the International Bureau in compliance with Rule 17.1(a) or (b)

World Intellectual Property Organization (WIPO) - Geneva, Switzerland
Organisation Mondiale de la Propriété Intellectuelle (OMPI) - Genève, Suisse

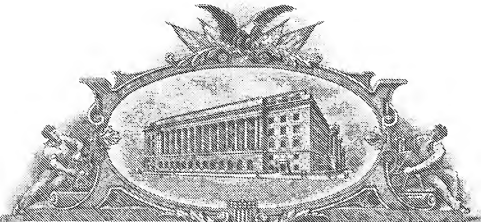

1383929

THE UNITED STATES OF AMERICA

TO ALL TO WHOM THESE PRESENTS SHALL COME:

UNITED STATES DEPARTMENT OF COMMERCE

United States Patent and Trademark Office

August 18, 2005

THIS IS TO CERTIFY THAT ANNEXED HERETO IS A TRUE COPY FROM THE RECORDS OF THE UNITED STATES PATENT AND TRADEMARK OFFICE OF THOSE PAPERS OF THE BELOW IDENTIFIED PATENT APPLICATION THAT MET THE REQUIREMENTS TO BE GRANTED A FILING DATE.

APPLICATION NUMBER: ***60/527,209***
FILING DATE: ***December 04, 2003***
RELATED PCT APPLICATION NUMBER: ***PCT/US04/40872***

Certified by

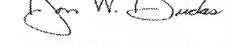

Under Secretary of Commerce
for Intellectual Property
and Director of the United States
Patent and Trademark Office

2

PTO/SB/16 (08-03)
Approved for use through 07/31/2006. OMB 0651-0032
U.S. Patent and Trademark Office; U.S. DEPARTMENT OF COMMERCE

PROVISIONAL APPLICATION FOR PATENT COVER SHEET

This is a request for filing a PROVISIONAL APPLICATION FOR PATENT under 37 CFR 1.53(c).

Express Mail Label No. EV240598931US

INVENTOR(S)		
Given Name (first and middle [if any])	Family Name or Surname	Residence (City and either State or Foreign Country)
John T	Groves	Berkeley, CA, US
Michael M.	Baksh	Fremont, CA, US
Michal	Jaros	Brno, CZ

Additional inventors are being named on the _____ *separately numbered sheets attached hereto*

TITLE OF THE INVENTION (500 characters max)

Phase Transitions and Molecular Detection in a Lipid Membrane - Derivatized Colloid

Direct all correspondence to: **CORRESPONDENCE ADDRESS**

[X] Customer Number: 08076

OR

[ ] Firm or Individual Name					
Address					
Address					
City		State		ZIP	
Country		Telephone		Fax	

ENCLOSED APPLICATION PARTS *(check all that apply)*

[X] Specification *Number of Pages* 43 [ ] CD(s), Number _____

[X] Drawing(s) *Number of Sheets* 10 [ ] Other (specify) _____

[ ] Application Data Sheet. See 37 CFR 1.76

METHOD OF PAYMENT OF FILING FEES FOR THIS PROVISIONAL APPLICATION FOR PATENT

[X] Applicant claims small entity status. See 37 CFR 1.27.

[ ] A check or money order is enclosed to cover the filing fees.

[X] The Director is hereby authorized to charge filing fees or credit any overpayment to Deposit Account Number: 120690

[ ] Payment by credit card. Form PTO-2038 is attached.

FILING FEE Amount ($)

80.00

The invention was made by an agency of the United States Government or under a contract with an agency of the United States Government.

[ ] No.

[X] Yes, the name of the U.S. Government agency and the Government contract number are: Department of Energy DE-AC03-76SF00098

Respectfully submitted,

SIGNATURE _____ Date 12/11/03

TYPED or PRINTED NAME David J Aston REGISTRATION NO. 28,051 *(If appropriate)*

Docket Number: IB-1919P

TELEPHONE 510-495-2839

USE ONLY FOR FILING A PROVISIONAL APPLICATION FOR PATENT

Phase Transitions and Molecular Detection in a Lipid Membrane – Derivatized Colloid

Michael M. Baksh, Michal Jaros, and John T. Groves

Statement of Governmental Support

This invention was made during work supported by the U.S. Department of Energy at Lawrence Berkeley National Laboratory under contract No. DE-AC03-76SF00098. The government has certain rights in this invention.

Background of the Invention

The molecular architecture of cell membranes is a unifying theme shared by all living organisms, and chemistry within the membrane environment is of widespread importance to humans. For example, a majority of known drugs and infectious disease agents target membranes. A significant challenge in the study of biochemical reactions on membrane surfaces is the presentation of a naturally fluid membrane environment within a context that facilitates detection and characterization of molecular interactions. One strategy, which has yielded insightful results, involves lipid membranes supported on solid substrates such as silica or certain polymers[1,2]. The membrane is firmly trapped near the solid interface, but retains the natural fluidity and significant biological functionality[3]. Supported membranes have been implemented with a variety of therapeutically valuable membrane proteins, including G protein-coupled receptors[4]. However, detection of molecular interactions on membrane surfaces generally requires elaborate techniques such as surface plasmon resonance (SPR)[5] or total internal reflection (TIR) microscopy[6], which additionally necessitates the use of fluorescent labels. Here, we examine colloidal phase transitions of membrane-derivatized silica beads as a label-free and essentially power-free method of revealing molecular interactions on lipid membrane surfaces.

The Mirkin references regarding current detection methods with colloidal particles:

1. 2000 Taton, T.A.; Mirkin, C.A.; Letsinger, R.L.; Scanometric DNA Array Detection with Nanoparticle Probes:
Science 289: 1757-1759

2. 2000 Reynolds, R.A.; Mirkin, C.A.; Letsinger, R.L.; Homogenous, Nanoparticle-Based Quantitative Colorimetric
Detection of Oligonucleotides: J. Am. Chem. Soc. 122: 3795-3796.

3. 1997 Elghanian, R. et. al.; Selective Colorimetric Detection of Polynucleotides Based on the Distance-Dependent Optical Properties of Gold Nanoparticles: Science 277: 1078-1081

Summary of the Invention

The invention comprises a method of detection using statistical analysis of the collective behavior of a population of bead particles after a binding event to achieve a phase transition at or near equilibrium. Using direct optical imaging, we observe multiple near-equilibrium phases and find that analyte binding to a bead surface at densities as low as 10^{-4} monolayer can trigger a phase transition. Statistical analysis of bead pair distribution functions enable quantitative comparison among different systems and reveals subtle, pre-transition effects and signature post-transition behavior. The binding event on the surface of a bead particle which achieves a phase transition at or near equilibrium should produce a recognizable signature effect on the random distribution of the beads that can be interpreted and calculated by statistical analysis.

In a first aspect, the invention contemplates bead particles formed from porous and nonporous forms of such materials as silica and silica-containing compounds, polymers such as polystyrenes, polymethacrylates, polyacrylates, polyacrylamides, polymethacrylamides and siloxanes, microgels and hydrogels, gold or other metals, Group II-VI materials, Group III-V materials, branched and unbranched compositions (e.g. dendrimer) and other inorganic and organic metals and materials.

These bead particles may be derivatized with an outer doped or undoped lipid membrane layer or derivatized with a ligand specific for an analyte. Suitable ligands include a wide range of materials or substances, including, but not limited to, proteins (e.g. antibodies, cytokines), small molecule drugs, larger polymeric drugs, peptides, protein therapeutics, nucleic acids, carbohydrates, phosphate and reactive groups, and inorganic or organic molecules and compositions.

In one aspect, the invention uses derivatized beads having an outer doped lipid membrane layer with a water layer in between. The lipid membrane is doped with 10^{-2} to 10^{-6} M concentrations of a protein or membrane-associated ligand. Protein or analyte binding to the membrane surfaces through the ligand cause the beads to undergo a phase transition and respond in a specific manner – i.e., the bead population goes from a condensed to dispersed population. Phases can be directly imaged and phase transition determined using the naked eye or a device that can detect the phase transition.

The disclosure specifically describes silica beads derivatized with a membrane, wherein the membrane is doped with a protein ligand which is specific for an analyte, such as toxins, hormones, enzymes, lectins, proteins, signaling molecules, inorganic or organic molecules, contaminants, antibodies, viruses and bacteria.

Description of the Invention

I. Introduction

Colloidal particles self-assemble into a variety of ordered phases and the study of colloidal phase transitions is currently an area of intensive activity[7]. This collective effort is fueled by the intriguing statistical thermodynamic behavior of colloids, their general applicability to the study

of phase transitions, and their important material properties, such as the ability to self assemble into ordered structures[8-12]. The behavior of a colloidal system is driven by the pair interaction potential between particles. In the case of membrane-derivatized silica beads, the pair potential is dominated by membrane-membrane interactions. Two-dimensional dispersions of lipid membrane-derivatized silica beads exhibit colloidal phase transitions that are governed by details of these membrane surface interactions. The collective phase behavior serves as a cooperative amplifier that produces a readily detectable response from a small number of molecular events on the membrane surface.

II. Bead Particle Compositions

Bead particles can be derivatized with coatings varying widely in composition, providing a precise method of adjusting the chemical and biological constitution of the surface. As shown schematically in Fig. 1a, beads settle gravitationally onto the underlying substrate when dispersed, and form a two-dimensional colloid. The beads exhibit free lateral diffusion and the system behaves as an ergodic fluid. Brownian trajectories can be predicted for beads. Bead diffusion coefficients are essentially independent of membrane composition or diameter size of beads and are ~80% as predicted by the Stokes-Einstein relation for purely viscous drag, indicating a small contribution from drag on the underlying substrate.

Depending on the strength of the interaction between membranes on the bead surfaces, dispersed (gas) or condensed (liquid or crystalline) phases of the colloid can be observed. Bead mobility is retained in condensed phases (Fig. 2b). The mobility of individual beads, in both condensed and dispersed phases, defines the rate of system equilibration. The time-scale of bead condensation onto and evaporation from the condensed crystallites, seen in Fig. 2b, can be rapid (e.g., several minutes) to more than half an hour. Additionally, the overall morphology and quantitative pair distribution functions of the phases should remain constant, despite the interchange of individual colloids.

These observations suggest that the system is near equilibrium, at least over length-scales of several bead diameters.

The beads can be comprised of various materials including porous and non-porous materials forms of such materials as silica and silica-containing compounds, polymers such as polystyrene, polymethacrylates, polyacrylates, diacetylenes, alkenes, thiophenes, polythiophenes, glycopolythiophenes, imides, acrylamides, acrylates, methacrylamides, methacrylates, vinylether, malic anhydride, urethanes, allylamines, siloxanes, anilines, pyrroles, and vinylpyridinium and other hydrogel polymeric materials, microgels and hydrogels, gold or other metals, Group II-VI materials, Group III-V materials, branched and unbranched compositions (e.g. demdrimer), other inorganic and organic metals and materials acetylenes.

It is contemplated that the beads can be from 10nm to 50μm in diameter. Preferred sizes of beads are about 1μm – 6.8μm diameter beads, but more preferably about 5μm – 6.8μm. In a preferred embodiment, 5μm – 6.8μm silica glass microspheres can be obtained commercially.

The chemical composition of the lipid membrane can be adjusted to modulate the pair interaction potential. Condensed phases or condensed aggregations, as seen in Fig. 2b, formed whenever the

coating membrane was net neutral or negatively charged. In contrast, net positively charged membranes led to dispersed phases or more random aggregations. The occurrence of multiple phases indicates that pair interaction energies poise the system near a phase transition. As such, small perturbations on the membrane surface are expected to induce significant changes in the macroscopic organization of the colloid. We observe this prediction by examining the effects of protein binding to membrane-associated ligands.

In one embodiment, bead particles can be derivatized with bilayer membranes varying widely in composition, providing a precise method of adjusting the chemical and biological constitution of the surface. Lipid membranes can be assembled on silica beads by essentially the same vesicle fusion process used to form supported membranes on monolithic substrates[13,14]. The resulting membrane, illustrated schematically in Fig. 1a, is continuous and retains lateral fluidity. Fig. 1b and c depict fluorescence recovery after photobleaching (FRAP) experiments performed on beads coated with fluid and nonfluid (gel state) membranes, respectively. Diffusion coefficients of 1 – 5 $\mu m^2/s$, as seen here, are typical of fluid membranes.

The membranes can generally be comprised of membrane components which can include, but are not limited to, lipids, cholesterols, steroids, ergosterols, polyethylene glycols, proteins, peptides, or any other molecules such as fatty acids, triacylglycerols, glycerophospholipids, sphingolipids (e.g. sphingomyelins, cerebrosides and gangliosides), sterols, cholesterol, surfactants, polysorbate, octoxynol, sodium dodecyl sulfate, zwitterionic detergents, decylglucoside, deoxycholate, diacetylene derivatives, phosphatidylserine, phosphotidylinositol, phosphatidylethanolamine, phosphatidylcholine, phosphatidylglycerol, phosphatidic acid, phosphatidylmethanol, cardiolipin, ceramide, lysophosphatidylcholine, D-erythrosphingosine, sphingomyelin, dodecyl phosphocholine, N-biotinyl phosphatidylethanolamine, and other synthetic or natural components of cell membranes that can be associated with a membrane or membrane assemblies such as liposomes and films.

In a preferred embodiment, the membrane is preferably comprised of a neutral and a negatively- or positively-charged lipid monomer, more preferably a neutral and a negatively-charged lipid. Suitable lipids can include, but are not limited to, phosphatidylserine, dipalmitoylphosphatidic acid, 1,2-Dimyristoleoyl-*sn*-glycero-3-phosphocholine(DMOPC), 1,2-dimyristoyl-*sn*-glycero-3-[phospho-L-serine] (sodium salt) (DMPS), and 1,2-dioleoyl-*sn*-glycero-3-ethylphosphocholine (DOEPC), distearoylphosphatidylglycerol, phosphatidylinositol, 1,2-dioleoyl-3-dimethylammonium-propane, 1,2-dioleoyl-3-trimethylammonium–propane, dimethyldioctadecylammonium bromide, 1,2-dioleoyl-*sn*-glycero-3-ethylphosphocholine, N-(7-nitrobenz-2-oxa-1,3-diazol-4-yl)-1,2-dihexadecanoyl-*sn*-glycero-3-phosphoethanolamine ammonium salt, and and N-1,2-dihexadecanoyl-*sn*-glycero-3-phosphoethanolmine triethylammonium salt, L-a-Phosphatidylcholine (Egg PC), Cholesterol, N-Dinitrophenylaminocaproyl Phosphatidylethanolamine (DNP-Cap PE), ceramides (natural and synthetic preparations), N-[12-[(7-nitro-2-1,3-benzoxadiazol-4-yl)amino]dodecanoyl]-Sphingosine-1-Phosphocholine (C12-NBD Sphingomyelin), 1,2-Dioleoyl-sn-Glycero-3-Phosphoethanolamine-N-(Cap Biotinyl), 1-Palmitoyl(D31)-2-Oleoyl-*sn*-Glycero-3-Phosphoinositol (and other Phosphoinositol extracts), and polyethylene glycols of various lengths.

LBNL Docket No. IB-1919P
Express Mail Label No. EV240598931US

In a preferred embodiment, the membrane is comprised of 1,2-Dimyristoleoyl-*sn*-glycero-3-phosphocholine(DMOPC), 1,2-dimyristoyl-*sn*-glycero-3-[phospho-L-serine] (sodium salt) (DMPS), and 1,2-dioleoyl-*sn*-glycero-3-ethylphosphocholine (DOEPC).

In a preferred embodiment, the bead particles are silica beads derivatized with a lipid membrane which is doped with protein ligand specific for an analyte. Upon binding an analyte, a disruption of the polymer backbone occurs, resulting in a detectable phase transition from condensed to dispersed.

Methods describing such doping of membranes are Joshua Salafsky, Jay T. Groves, and Steven G. Boxer,"Architecture and Function of Membrane Proteins in Planar Supported Bilayers: A Study with Photosynthetic Reaction Centers", *Biochemistry*, 35, 14773-14781 (1996); and Jay T. Groves, Christoph Wülfing, and Steven G. Boxer, "Electrical Manipulation of Glycan-Phosphatidyl Inositol-Tethered Proteins in Planar Supported Bilayers", *Biophysical Journal*, 71, 2716- 2723 (1996)and are hereby attached and incorporated by reference. The first reference depicts a system where a protein is actually incorporated directly into the membrane, while the second reference depicts a system where the protein is bound to a GPI-linker that is incorporated into the membrane.

In an alternative embodiment, the beads can be derivatized with coating comprising membrane components which may or may not be comprised of lipids or a ligand. This contemplates the alternative embodiment wherein the coating itself acts as a ligand, or the ligand is directly coupled to the beads.

The ligand groups of the present invention can be comprised of a wide variety of materials. The main criterion is that the ligand has a specific affinity for the analyte of choice. Appropriate ligands include, but are not limited to, carbohydrates, nucleic acids, biotin, streptavidin, peptides, proteins, lipoproteins, glycoproteins, enzymes, receptors, channels, antibodies, drugs, chromophores, antigens, chelating compounds, molecular recognition complexes, ionic groups, polymerizable groups, dinitrophenols, linker groups, electron donor or acceptor groups, hydrophobic groups, hydrophilic groups, or any organic molecules that bind to receptors. Additionally, multiple ligands can be incorporated. As is clear from the broad range of ligands that can be used with the present invention, an extremely diverse group of analytes can be detected.

III. Detection Assay

The invention comprises a method of detection using statistical analysis of the collective thermodynamic behavior of a population of bead particles after a binding event to achieve a phase transition at or near equilibrium. The present method provides a method of detection of the binding of an analyte to a ligand on a bead surface. The binding of the analyte to the beads of the invention trigger a phase transition (e.g. condensed to dispersed or dispersed to condensed).

This method of detection requires no power, but relies on the thermodynamic behavior of a population of bead particles having a bead size and surface composition that is positioned close to a phase transition, and the solution that the assay is performed in. The binding event and

subsequent detection does not have to occur at a phase transition, however, at this point is where the assay is at maximum sensitivity.

Using direct optical imaging, we observe multiple near-equilibrium phases and find that analyte binding to a bead surface which can trigger a phase transition affects the aggregation, distribution and behavior of the bead particles in relation to each other. Statistical analysis of bead pair distribution functions enable quantitative comparison among different systems and reveals subtle, pre-transition effects and signature post-transition behavior. The binding event on the surface of a bead particle which achieves a phase transition at or near equilibrium should produce a recognizable signature effect on the random distribution of the beads that can be interpreted and calculated by statistical analysis.

The distribution of the population of beads can be expressed in terms of the paid correlation and the phase transition can be mapped by analyzing the functions. The minimum population number is 2, preferably at least 10, more preferably 1000.

Fig. 3 depicts a time sequence of a phase transition triggered by addition of protein at $t = 0$ s (Fig. 3a top left panel). Within seconds of adding a drop of a solution containing an analyte to the top of the well, uniform disruption of the condensed phase is discernable (Fig. 3a top right panel). At about a minute, the colloid should attain a dispersed distribution (Fig. 3a bottom panels). Individual bead mobility is unaffected by protein binding, so exposure to a particular analyte of interest should trigger a phase transition only when the appropriate cognate ligand has been incorporated into the colloid membrane. The physical presence of the analyte bound to the membrane surface increases the closest approach position between two membranes [15] and, correspondingly, reduces the cumulative strength of the van der Waals attraction between beads, enabling the phase transition.

Quantitative analysis of the colloidal phases was performed by extracting the pair distribution function, $g(r)$. Bead positions were measured from wide-field (~1 mm^2) images by an object locating algorithm to a precision of ~16 nm. Wide field images of large populations of beads should be taken with a high resolution camera such as a charged-coupled device camera and analyzed with imaging software such as METAMORPH (Universal Imaging Corporation, Cranberry Township, PA). Using such software, the centers of beads can be found very accurately using intensity because the beads are spherical clear objects. The X,Y coordinates of the center of each bead are calculated for each image to calculate the distances between the center of each bead and the centers of its nearest neighboring beads, second nearest neighbors and third nearest neighbors, etc.

For a finite rectangular window of spatial dimensions X by Y, $g(r)$ can be computed from

(Equation 1) $$g(r) = \frac{\eta(r) X^2 Y^2}{N(N-1)\delta r\left[\pi XYr - 2(X+Y)r^2 + r^3\right]}$$

where $\eta(r)$ is the number of bead pairs with separation distance $r \pm \delta r/2$ (δr = 40 nm for the data presented here), r is the radius of beads used and N is the total number of beads.

The number of iterations for a $g(r)$ plot for effective analysis depends on N, the number of bead pairs analyzed. If N=1, to calculate g(r) to satisfaction may require a very long course of time in order to gather enough data to show the particular $g(r)$ plot for that particular composition of beads. Therefore it is preferred that N is at least 10, preferably 1000 or more to gather sufficient data in a matter of seconds.

Plots of $g(r)$ during a phase transition triggered by analyte binding are illustrated in Figure 7B. The condensed phase $g(r)$ is characterized by a large peak at the nearest neighbor separation distance of one bead diameter (r_0) and secondary peaks occurring at $r = \sqrt{3}r_0$ and $2r_0$, corresponding to next nearest neighbors in the hexagonal crystallites. In Fig. 7B, the first peak is found at r=5μm, the second peak corresponding to distance to the second nearest neighbors is found at around 7μm, and the peak corresponding to the distance to the third nearest neighbors is found at around 10μm.

Referring to Fig. 3B, plots of $g(r)$ for different time points during a phase transition triggered by protein binding are shown. The condensed phase $g(r)$ is characterized in the red curve at t=0 by a large peak at the nearest neighbor separation distance of one bead diameter (r_0) and secondary peaks occurring at $r = \sqrt{3}r_0$ and $2r_0$, corresponding to next nearest neighbors in the hexagonal crystallites. Independent measurements of $g(r)$ were highly consistent. Standard deviations in the magnitude of the r_0 peak determined from separate colloidal preparations were generally less than 5%. Dispersed phases, consisting of random distributions and correspondingly flat $g(r)$ functions, are visibly distinguishable from condensed phases. (See blue, black, and green curves at times 30, 60 and 240s). Quantitative determination of $g(r)$ additionally distinguishes a range of intermediate distributions. These can be transient, such as the dispersing crystallites in Fig. 3a, t = 30s. Intermediate degrees of order were also observed in near equilibrium distributions, corresponding with differing amounts of protein binding on the membrane surface.

Quantitative analysis of the colloidal phases can further be performed by extracting an infinite series of distributions. This is used when the number of bead particle types is greater than 1. See the examples describing analysis of heterogeneous mixtures of beads.

For quantitative comparison among samples, we isolate the first peak in $g(r)$, which occurs at the particle diameter (5μm), and compute the corresponding effective interaction energy, E_i. E_i is an approximation of the k_BT energy and calculated by taking the natural log of the height of the first peak in the g(r) plot and either fitting it to a curve having a known function or expression, or by integrating the area under the curve. This allows precise comparison among samples containing equal area fractions (φ) of beads and E_i converges to the pure pair interaction energy at low coverage densities. Although equilibrium is required for E_i to have meaningful units of energy, this is not a requirement for effective comparison. As long as each colloidal system is cast in an initially uncorrelated state, nonequilibrium distribution measurements at defined time intervals can also be used for quantitative comparison.

While the calculation of E_i may be useful, it is contemplated that it may not be necessary in cases of detection such as that exemplified in Fig. 5C. The qualitative $g(r)$ plots show a very distinctive missing first peak when the analyte is detected and bound by the beads being analyzed.

At equilibrium, $g(r)$ is physically related to the potential of mean force, $w(r)$:

(Equation 2) $$g(r) = e^{-w(r)/k_BT}$$

In dilute systems, $w(r)$ is equivalent to the pair interaction potential and thus provides a direct measure of the interaction energy. In more concentrated systems, $w(r)$ includes effects due to neighboring particles. In principle, $w(r)$ can be deconvolved to obtain the true pair potential using the Ornstein – Zernike integral equation along with an appropriate truncating approximation, such as the Percus – Yevick equation(24, 25). However, this is not necessary for the present purposes.

Independent measurements of $g(r)$ should be highly consistent. Standard deviations among E_i values determined from separate colloidal preparations from the same starting materials were generally less than 0.1 k_BT.

Precise measurement of $g(r)$ provides a means to explore subtleties of the interactions between different membrane compositions. We examine the transition from condensed to dispersed phases as the net electrostatic charge of the membrane is gradually adjusted from negative to positive. Figure 4 illustrates results from a panel of membrane compositions with completely ionized charge densities ranging from -1.43 x 10^4 to 7.15 x 10^4 e/μm^2 per membrane leaflet; actual surface charge densities are expected to be significantly lower due to incomplete ionization. Strongest interactions are seen for the beads derivatized with neutral membranes. This is consistent with the minimization of electrostatic repulsion expected between neutral surfaces. Away from neutrality, E_i falls off rapidly for the positively charged membranes whereas only a slight, but consistent, reduction is observed as the membranes become negatively charged. The DMPS membranes used in the protein binding experiments (-1.43 x 10^5 e/μm^2 at complete ionization) exhibit E_i similar to that of the neutral membranes (~2 k_BT, see Figure 3).

Several forces, including van der Waals, steric-hydration, and electrostatic contribute to the interaction potential between membranes. Forces between lipid membranes supported on molecularly flat mica surfaces have been studied using the surface forces apparatus (SFA)(26). Under conditions resembling those of our colloid experiments, adhesive interaction energies between mica – supported membranes are of order ~10^{-22} J/nm^2 at the minimum separation of ~0.5 – 1 nm(27, 28). This is in general agreement with predictions of Derjaguin-Landau-Verwey-Overbeek (DLVO) theory, except for the minimum separation distance, which is determined largely by repulsive steric-hydration forces. We calculate the DLVO interaction potential between membrane-derivatized beads using the linearized Derjaguin approximation for electrostatic interactions and the non-retarded van der Waals potential between two spheres(20) with Hamaker constant = 7 x 10^{-21} J (28). The van der Waals attraction is strong (350 k_BT at 1 nm minimum separation) and is balanced by electrostatic repulsion, which rapidly becomes dominant at surface potentials of magnitude ≥ 14 mV (1 nm minimum separation). The large overall magnitude of the DLVO interaction suggests it is improbable that a precise balance between van der Waals and electrostatic forces could lead to the consistently weak adhesion we observe experimentally.

A plausible explanation of the experimental results may be constructed based on the fact that the membrane-derivatized (acid-etched) silica beads are not molecularly flat. As two beads approach one another, regions of relatively higher surface topography will experience shorter interaction distances. Details of the contact geometry between rough surfaces will produce differential effects on the various inter-particle forces, based on the characteristic length scales over which they act. For example, surface topography on the nanometer length scale is expected to have little effect on electrostatic interactions due to the long Debye lengths (>100 nm) in these experiments. In contrast, the short-range van der Waals interaction is strongly modulated by nanometer-scale surface topography: most of the adhesive energy will come from the small fractional area of the surfaces in closest contact. The similarly short range steric-hydration forces will determine the minimum separation distance between two beads based on the these close contact regions as well. Large surface areas are thus precluded from experiencing short–range interaction forces due to surface topography.

Analyte binding to the membrane surface creates topography and changes the effective roughness. This suggests a possible mechanism for the analyte binding – induced colloidal phase transition in which the presence of a few proteins on the membrane surface shifts the closest approach position between two beads and, correspondingly, modulates the cumulative strength of the van der Waals attraction(29, 30). The experimental ability to modulate the interaction energy by adjustments in the membrane composition is of practical importance for the design and optimization analytical systems based on this type of colloidal phase transition.

The detection assay of the analyte can be performed in a high throughput manner due to the scalability and the low cost of the detection. A software program was written to automate the calculation of $g(r)$. The program is inputted text files containing X,Y coordinate positions of each bead in each image. The software also takes into account such parameters such as pixel resolution of each image, size of beads, size of the image window, and desired resolution of $g(r)$. $g(r)$ can be resolved at high or low resolutions, however, it is preferred that $g(r)$ be resolved at higher resolutions such as 0.04 because this has acceptable signal to noise ratio. If the resolution is lower, such as at 0.01 or lower resolutions, then there is likely too much noise. The program calculates and outputs the g(r) plot. Experiments were generally carried out at bead area fractions of $\phi \approx 0.15$-0.25, corresponding to ~7000 individual beads per image, where ϕ is the area of the window covered by beads, as opposed to the empty spaces between and around beads. Generally, about 5-10 independent images were averaged to generate $g(r)$ from $>10^8$ measured pair distances.

The imaging of the field areas can be automated, as long as the pictures are taken consistently, with the only limitation being the speed of the automated camera, software and hardware. The $g(r)$ plots may be generated fairly quickly so long as a sufficient number of beads are imaged over a sufficient time period.

It is further contemplated that the assay may be carried out with only such devices as a spectrophotometer or scanning plate reader that images or calculates light scattering in all wavelengths and spectra), to facilitate high throughput detection. The optical density of the particular bead population before the phase transition and at each phase transition is measured to

capture the signature optical density reading. Upon addition and binding of an analyte to the derivatized beads, the plate can be scanned for whether or not a phase transition has been triggered.

Other factors in the detection assay include the hydration layers, coatings, and the charge of the materials that the assay is carried out in. It is presently contemplated that the detection assay is preferably carried out in a Corning COSTAR 96-well 3997 polystyrene plate or a comparable high throughput plate. The assay can be feasibly carried out in 96-, 384- or 1536-well plates.

IV. Further Description of the Invention

The present invention concerns the detectability of phase transitions of particles (also referred to as beads, although they are not necessarily spherical) coated with ligands. The phase transition referred to herein is the phase from a liquid state (condensed) to a gaseous state (dispersed). The two states are distinguished by the clumping or the separateness of the particles, as detected and measured optically or by other means. By designing the system so that the particles are near the transition point between phases, small perturbations in binding of the particles to analytes can trigger a phase transition, preferably, as illustrated herein, a transition from condensed to dispersed.

The phase transitions are further illustrated in Figs. 2 and 3. In Fig. 2b, a single particle, identified by an arrow, may be seen to migrate with time into a cluster, into a stand alone position, and back into a cluster. This shows that the beads are in effect in a liquid, *i.e.* the particles are free to move about and change relative positions. The bottom two panels of Fig. 3b show a dispersed state, wherein the vast majority of particles stand alone. The actual degree of dispersion may be calculated and represented graphically, as shown in Fig 3b, discussed below. The degree of dispersion in a dispersed state may be thought of as a random location for any individual bead.

The preferred particles are inert beads, used in concentrations that yield, when the beads are arrayed on the bottom of a well or plate, an area fraction of 0.15 to 0.25, or as high as 0.45, *i.e.* 45 percent of the area is occupied by beads as opposed to spaces between or around beads. More beads will tend to make the assay more sensitive.

The beads should be large enough to be handled in the coating operation and small enough to have collective behavior, preferably 1- 10μm in diameter. Larger beads will be able to sense weaker interactions between the ligand and the analyte.

In order to study a biological system, the beads are preferably prepared with a lipid bilayer coating, in which the ligands are inserted. The lipid layer should be fluid, in order to allow the ligands and the lipids to diffuse around the bead. In order to mimic a cellular membrane, the lipids should be a mixture of neutral (e.g. DMOPC) and negatively charged lipids, although positively charged lipids such as DOEPC will also work. Preferably, about 10% of the lipids are negatively charged.

The ligands are inserted into the lipid coating at concentrations of between 10^{-2} to 10^{-4} molar, as illustrated below, although concentrations as low as 10^{-6} molar could be used in a system designed for low particle concentrations.

However, it should be realized that the present invention is not limited to lipid or cell membrane structures. Assays according to the teachings herein may be constructed by directly coupling ligands to the beads. Ligands such as antibodies or antibody binding fragments (Fab or FAB2, single chain antibodies, etc) may be coupled to silica, styrene, magnetic, or semiconductor nanocrystal beads to provide detection directed assays.

Referring now to Fig. 3b, a quantitative representation of the degree of dispersion is illustrated as a function of *g(r)*, which is a probability function, versus r, which is a distance between two beads. Thus, there are very few beads less than 10 μm apart, since this space is occupied by the diameters of the beads. Next, there is a peak in the vicinity of 15-20 μm if the beads are clumped together. One may take the integral of that first peak (shown at its highest at time 0) and measure the amount of analyte bound to the beads. Transition between a condensed state and a dispersed state is shown in the smaller peaks such as in Fig. 4 a, at ligand concentration 1E-4. Fig. 4a also demonstrates, that for this experiment, a ligand concentration of at least 1E-4, preferably 1E-3 is necessary to achieve a dispersed state.

A graphical representation of the curves shown in Figs 3, 4, 5 and 6 is set forth in Fig. 7B. It is shown that in a given clump or cluster of beads, the shortest distances shown at the top of the illustrated cluster will be quite numerous. The next nearest distances, shown as the lines in the bottom cluster, will also be present, but not as numerous. Note that the illustrated total cluster generates a curve similar to the experimental figures.

The curves are generated by using optical detection means (imaging software with a microscope as shown in Fig. 7A) to detect the location of each bead in a given area. Typically about 10^4 beads are imaged and positioned by x,y coordinates. The software then calculates, pairwise, the distance between the centers of every bead in the sample ($>10^8$ measurements). The number of distances is then plotted as shown in Fig. 7B and the other Figures.

IV. Applications

The bead particles of the preferred embodiment provide a sensitive, low-cost method of detecting analytes in any given solution. In the preferred embodiment, detection of the binding event to the ligand is used to detect pathogenic organisms, disease, toxins, contaminants, presence of a hormone, signaling molecule, antibody, cancer or a medical condition. In some embodiments, ligands are incorporated to detect a variety of pathogenic organisms including, but not limited to, sialic acid to detect HIV, *Chlamydia*, *Neisseria meningitidis*, *Streptococcus suis*, *Salmonella*, mumps, newcastle, and various viruses, including reovirus, Sendai virus, and myxovirus; and 9-OAC sialic acid to detect coronavirus, encephalomyelitis virus, and rotavirus; non-sialic acid glycoproteins to detect cytomegalovirus and measles virus; peptide sequences to hybridize to and identify the presence of *Anthrax*, CD4, vasoactive intestinal peptide, and peptide T to detect

HIV; epidermal growth factor to detect vaccinia; acetylcholine receptor to detect rabies; Cd3 complement receptor to detect Epstein-Barr virus; β-adrenergic receptor to detect reovirus; ICAM-1, N-CAM, and myelin-associated glycoprotein MAb to detect rhinovirus; polio virus receptor to detect polio virus; fibroblast growth factor receptor to detect herpes virus; oligomannose to detect *Escherichia coli*; ganglioside G_{M1} to detect *Neisseria meningitidis*; and antibodies to detect a broad variety of pathogens (*e.g.*, *Neisseria gonorrhoeae*, *V. vulnificus*, *V. parahaemolyticus*, *V. cholerae*, and *V. alginolyticus*).

The membrane-derivatized colloidal system introduced here has potential applications to a broad set of problems involving chemical events on cell membrane surfaces. These range from mapping ligand interactions with numerous cell surface proteins to detection of membrane-targeting bacterial toxins (e.g. botulism, cholera, anthrax, tetanus) and viruses. Membrane-derivatized beads can be combined in heterogeneous mixtures or with live cells (e.g. rosetting), allowing the methodology outlined here to be applied to analysis of intermembrane receptor-ligand interactions. Implementation of the colloid assay is amenable to automated liquid handling and imaging systems. Detailed analysis of spatial distribution functions, such as the pair distribution studied here, enables characterization of subtle interactions, including those which may not produce qualitatively recognizable effects. At the same time, the use of membrane coatings on colloidal particles offers an extensive repertoire of chemical functionality, which may prove valuable in non – biological settings. We anticipate that the general principles illustrated with lipid membranes in this work could be extended to other materials, such as the recently developed polymer vesicles[16].

Heterogeneous mixtures of beads can be used to examine interactions between membranes and/or membrane-associated ligands, or as a way of multiplexing. In this implementation, the beads could be individually identifiable with a label. The labels that can be used include, but are not limited to, fluroresrcent molecule doped into a bead material, fluorescent molecules doped into a membrane, semiconductor nanocrystals doped into bead material, etc. Strongly interacting beads of hereogeneous composition and functionality can be used as building lcoks for assembly into complex, multi-functional, nanoscale structures that can be used analysis of more complicated systems.

Beads can be mixed with live cells to quantitatively observe cell activation and proliferation (e.g. cell rosetting), or examine cellular interactions and multiplexing by creating a readily observable, controllable interface which retains cell-like properties.

Beads can also be functionalized internally with materials such as fluorescent labels, semiconductor nanocrystals, nano-scale detection devices, or custom –designed nanocrystals or molecules.

Bead particles can be dispersed into many different environments such as the human body, areas where extreme toxics or caustics are present, or hard vacuum settings, to detect the presence of a contaminant for example. The binding event is allowed to occur, then the beads are collected, then subjected to conditions which allow the assay to be performed. Since the beads settle and only a finite number of beads having undergone the binding event must be collected, the beads can be dispersed in even such environments as a flowing body of water, e.g. a river. For

example, the observable behavior and distribution of the beads after exposure to the river are compared with beads prior to casting in the river.

"Sensor" beads, exposed to the media under detection, can be moved through a plurality of background beads not exposed to the media. Phase data regarding the behavior of the bead particle can be elicited by observing the tracks of the relatively few "sensor" beads rather than looking at the overall spatial data of observing many beads in a finite location.

Example 1
Detection Assay using Silica Beads Derivatized with Ganglioside Doped Membranes

Membrane-derivatized silica beads were dispersed, underwater, where they settled gravitationally onto the underlying substrate and form a two-dimensional colloid. The beads exhibited free lateral diffusion and the system behaved as an ergodic fluid. Brownian trajectories for a dilute collection of beads are illustrated in Fig. 2a. Bead diffusion coefficients were essentially independent of membrane composition; measurements ranged from 0.079 to 0.086 $\mu m^2/s$ for 5 μm diameter beads. These values are ~80% that predicted by the Stokes-Einstein relation for purely viscous drag, indicating a small contribution from drag on the underlying substrate. Depending on the strength of the interaction between membranes on the bead surfaces, dispersed (gas) or condensed (liquid or crystalline) phases of the colloid were observed. Bead mobility was retained in condensed phases (Fig. 2b). The mobility of individual beads, in both condensed and dispersed phases, defines the rate of system equilibration. The time-scale of bead condensation onto and evaporation from the condensed crystallites, seen in Fig. 2b, was rapid compared to that of our experiments (several minutes vs. more than half an hour). Additionally, the overall morphology and quantitative pair distribution functions of the phases remained constant, despite the interchange of individual beads. These observations suggest that the system is near equilibrium, at least over length-scales of several bead diameters.

The chemical composition of the lipid membrane was adjusted to modulate the pair interaction potential and is described below. Condensed phases, as seen in Fig. 2b, formed whenever the coating membrane was net neutral or negatively charged. In contrast, net positively charged membranes led to dispersed phases. The occurrence of multiple phases indicated that pair interaction energies poise the system near a phase transition. As such, small perturbations on the membrane surface are expected to induce significant changes in the macroscopic organization of the colloid. We observe this prediction by examining the effects of protein binding to membrane-associated ligands.

Several protein systems were studied: antibody binding membrane surface antigen and bacterial toxins, cholera (CTB) and tetanus (TT), binding their respective membrane ligands, monosialoganglioside G_{M1} and trisialoganglioside G_{T1B}. Beads coated with 9% phosphatidylserine/91%DMOPC membranes were prepared as described in Example 2.

The beads thus prepared formed condensed phases, consisting of short-lived crystallites, for all membrane surface ligands studied. In all cases, protein binding to membrane surfaces triggered a condensed to dispersed phase transition. Fig. 3 depicts a time sequence of a phase transition

triggered by addition of protein at $t = 0$ s. These experiments were performed with ~300 μl solution in ~5 mm round wells of a 96-well plate. Within 30 s of adding a drop of protein solution to the top of the well, uniform disruption of the condensed phase was discernable. Within 60 s, the colloid attained a dispersed distribution. Individual bead mobility is unaffected by protein binding. Exposure to a particular protein of interest triggered a phase transition from condensed to dispersed phase only when the appropriate cognate ligand was incorporated into the colloid membrane. The physical presence of protein bound to the membrane surface increases the closest approach position between two membranes[15] and, correspondingly, reduces the cumulative strength of the van der Waals attraction between beads.

Example 2
Methods and Materials for Detection Assay using Silica Beads Derivatized with Ganglioside Doped Membranes

Materials: Lipids were obtained from Avanti Polar Lipids. 1,2-Dimyristoleoyl-*sn*-glycero-3-phosphocholine(DMOPC), 1,2-dimyristoyl-*sn*-glycero-3-[phospho-L-serine] (sodium salt) (DMPS), and 1,2-dioleoyl-*sn*-glycero-3-ethylphosphocholine (DOEPC) were received in chloroform and stored at –20°C for up to two weeks. Monosialoganglioside G_{M1}, bovine-ammonium salt (G_{M1}) was received from Matreya Inc. in powder form and dissolved in 2:1 chloroform/methanol to 1mg/mL for storage at –20°C. Trisialoganglioside G_{T1B}, bovine brain (G_{T1B}) was received from Sigma in powder form and dissolved in 2:1 chloroform/methanol to 1mg/mL for storage at –20°C. The fluorescent probe *N*-(Texas red sulfonyl)-1,2-dihexadecanoyl-*sn*-glycero-3-phosphoethanolamine, triethylammonium salt (Texas Red® DPPE) was purchased from Molecular Probes in powder form and dissolved in chloroform before use. Cholera toxin subunit B (CTB), FITC labeled, was purchased from Sigma, dissolved in 0.2xPBS to a concentration of 0.5mg/mL and stored at 4°C. Unlabeled α-Bungarotoxin (BT) was purchased from Sigma, dissolved in 0.2xPBS to a concentration of 0.5mg/mL and stored at 4°C. Tetanus toxin, c-fragment (TT), fluorescein labeled, was purchased from Calbiochem, reconstituted in sterile H_20 to a concentration of 0.1mg/mL TT and 10mM sodium phosphate buffer, and stored at 4°C. Bovine fetal calf serum (FCS) was purchased from Sigma, reconstituted in sterile H_20 and stored at 4°C. Unlabeled rabbit IgG fraction antibodies anti-Texas Red®, were purchased from Molecular Probes at a concentration of 1mg/mL and stored at 4°C. 5 μm mean diameter silica glass microspheres were obtained from Bangs laboratories and stored at 4°C under DI H_20.

Supported Membranes: Supported bilayers were formed by fusion of small unilamellar vesicles (SUV) onto clean glass microspheres. A lipid solution in chloroform was evaporated onto small round-bottom flasks and hydrated for an hour at 4 °C in 18.2 MΩ-cm water at ~3.3mg/mL. The lipids were probe-sonicated to clarity in an ice-water bath and untracentrifuged for 2 h at 160,000 g and 4°C. The supernatant was stored at 4°C for up to one week. Glass surfaces were prepared for deposition by boiling at 250°C in concentrated nitric acid followed by extensive rinsing. Bilayers were allowed to self-assemble on the microbead surface by mixing equal amounts (100μL) of spreading solution (1:1 SUV/PBS) and microbead solution together in a 1.5mL centrifuge tube. Excess vesicles were removed by pelleting the microbeads via pulse-centrifugation and removal of the supernatant. 1mL of 18.2 MΩ-cm water was then added to the pelleted microbeads and the entire mixture vortexted to allow resuspension.

Colloid Formation: Colloids were cast by diluting the microbead suspension to desired concentrations and pipetting 200-300 μL of the suspension into Costar number 3997 96-well plates. The 96-well plates were left undisturbed for 15 minutes to allow even settling of the microbeads to the bottom of each well.

Protein Binding: Protein binding to the colloid membrane was accomplished in two ways. Protein solution was added to pre-formed colloid dispersions by pipetting a ~5μL droplet of protein solution into ~300 μL in a well of a 96-well plate with the 2-D colloid formed at the bottom. Alternatively, protein solution could also be incubated with the microbead suspension for a given length of time, and this solution then pipetted into a well of a 96 well plate to cast the colloid, as described above.

Anti-Texas Red® rabbit IgG fraction antibodies were bound to Texas Red®-containing membranes by incubating a 20μg/mL solution of the antibody with 1mL of the bead solution for 45 minutes in the dark at room temperature, vortexing gently every 5 minutes. Antibodies were also bound to Texas Red®-containing membranes by adding antibody solution directly to the cast colloid in the 96-well plates. Bacterial toxins (CTB, TT, BT) were bound to membranes (containing either G_{M1}, G_{T1B}, or no ganglioside) by incubating the toxins at varying concentrations with bead solution for 50 minutes in the dark at room temperature, under continuous, gentle mixing.

Imaging: Supported bilayer-coated microbeads were diluted to a working concentration and deposited onto Corning 96-well cell culture clusters for viewing. Microbeads were viewed at room temperature with a Nikon TE-300 inverted fluorescence microscope (Nikon, Japan) equipped with a mercury arc lamp for fluorescence and a 100W halogen lamp for brightfield illumination. Images were recorded with a Roper Scientific CoolSnap HQ charge-coupled device camera (Roper Scientific CoolSnap HQ, USA). Images were acquired with SIMPLE PCI (Compix Inc., Cranberry Township, PA) and analyzed with METAMORPH (Universal Imaging Corporation, Cranberry Township, PA).

Data Analysis: To obtain Equation (1), in the text, the pair distribution function is expressed as $g(r) = n(r)/p(r)$, where $n(r) = 2\eta(r)/(N(N-1)\delta r)$ is the actual relative density of bead pairs with separation distance r (see text for definitions of other symbols) and $p(r) = 2(\pi XYr - 2(X+Y)r^2 + r^3)/(X^2Y^2)$ is the general probability density of finding a bead pair with separation distance r in a finite rectangular window of spatial dimensions X by Y. To obtain this expression for $p(r)$, we solve the line integral $p(r) = \int_Q p(r_x)p(r_y)dq$, where $p(r_x) = 2(X - r_x)/X^2$ and $p(r_y) = 2(Y - r_y)/Y^2$ are probability densities of finding a bead pair with r_x and r_y absolute projections of the separation vector $\boldsymbol{r}$, respectively, and Q is the all-positive quarter of a circle.

At equilibrium, g(r) is physically related to the potential of mean force, $w(r)$: $g(r) = e^{-w(r)/k_BT}$. In dilute systems, $w(r)$ is equivalent to the pair interaction potential and thus provides a direct measure of the interaction energy. In more concentrated systems, $w(r)$ includes effects due to neighboring particles. For quantitative comparison among samples, we isolate the

first peak in $g(r)$, which occurs at the particle diameter, and compute the corresponding effective interaction energy, E_i. This allows precise comparison among samples containing equal area fractions (ϕ) of beads and E_i converges to the pure pair interaction energy at low coverage densities. Although equilibrium is required for E_i to have meaningful units of energy, this is not a requirement for effective comparison. As long as each colloidal system is cast in an initially uncorrelated state, nonequilibrium distribution measurements at defined time intervals can also be used for quantitative comparison. Independent measurements of $g(r)$ were highly consistent. Standard deviations among E_i values determined from separate colloidal preparations from the same starting materials were generally less than 0.1 k_BT.

Example 3
Detection using Derivatized Bead Particles to Detect Cholera and Tetanus toxins

Measurements of near equilibrium colloidal distributions over a range of protein and ligand concentrations were performed to explore the utility of the phase transition as a readout of protein binding on membrane surfaces. Antibody studies were performed using a monoclonal IgG antibody that binds the fluorescent membrane probe, Texas Red-DPPE. Samples incubated with 20 μg/ml anti-Texas Red antibody exhibit a clear transition from condensed to dispersed phases for ligand surface concentrations $\geq 10^{-4}$ monolayer (Fig. 4a). This corresponds to ~10 ligand molecules on each membrane within the contact region where intermembrane separations are < 10 nm (5 μm beads). For bacterial toxin binding studies, the ganglioside ligands G_{T1B} or G_{M1}, were incorporated into membranes at a constant 0.5%. Incubation with TT triggered formation of a dispersed phase in the G_{T1B}-containing colloid while no effect was produced in the G_{M1} colloid (Fig. 4b). Analogously, exposure to CTB triggered the transition to a dispersed phase in the G_{M1} colloid without producing any effect on the G_{T1B} colloid (Fig. 4c). Exposure to Bungarotoxin (1 μM) produced no effect in either colloid. The magnitude of the r_0 peak in the measured $g(r)$ traces the surface concentration of bound protein.

CTB – G_{M1} and TT – G_{T1B} binding was characterized by incubating planar supported membranes (formed by depositing SUV's onto glass coverslips) with varying concentrations of CTB and TT and monitoring fluorescence from either the the FITC label (from CTB) or the fluroescein label (from TT). Results indicate that CTB binds the 89% DMOPC/ 9% DMPS/ 1% G_{M1}/ 1% Texas Red DPPE membranes studied here with an effective dissociation constant of ~41 nM (see Figure 5A). Since CTB – G_{M1} binding is not monovalent, this is an approximate representation of the binding affinity. Results indicate that TT binds the 89% DMOPC/ 9% DMPS/ 1% G_{T1B}/ 1% Texas Red DPPE membranes studied here with an effective dissociation constant of ~60 nM (see Figure 5B).

Realistic detection experiments were performed by mixing FCS (0.1%) and CTB (at a 100nM concentration) in a sample of river water containing approximately 4mg/mL of organic and inorganic components. The mixture was filtered with a 0.2μm filter and incubated with 1mL of the bead solution solution for 50 minutes in the dark at room temperature, continuously mixing gently. Excess soluble components were removed by rinsing the mixture with 18.2 MΩ-cm water prior to casting the colloid.

Supporting Table 1 in Fig. 5B contains results for a series of experiments designed to test the selectivity of the colloid detection scheme. Beads derivatized with membranes containing G_{M1}, G_{T1B} or no ganglioside were tested for binding affinity against CTB, TT and BT. The resulting colloidal distribution is evaluated in terms of an effective interaction energy, E_i, as defined below. It is observed that in the absence of any type of toxin, beads derivatized with any of the three types of membranes had E_i values greater than ~2. This value is representative of a condensed phase and is considered a negative signal. In the presence of a toxin and its specific target (G_M -CTB, G_{T1B} -TT), the E_i value for the colloid was less than ~1 (shown in red). This value is representative of a colloid in a dispersed phase and is considered a positive signal. In addition, specificity is explicitly shown with toxins in the presence of incorrect or nonexistent targets. Negative signals were obtained for the follwing systems: G_{M1} -TT, G_{T1B} - CTB, CTB and TT with no target, and BT with all three membrane types.

G(r) plots for all of this data are present in Fig. 5C. Insensitivity to a wider variety of potential targets was demonstrated by incubating 0.1% fetal calf serum (FCS) in the presence of a G_M-containing membrane. The E_i value of the resulting colloidal distributuion was greater than ~2, indicative of a negative signal. Notice that when CTB is present and binds to the beads derivatized with the G_{M1}-containing membrane, the first peak in the $g(r)$ plot is noticeably absent. And when the toxin to be detected is tetanus toxin, there is a noticeably absent peak in the $g(r)$ plot for beads derivatized with G_{T1B} –containing membranes. Thus, the $g(r)$ plots can qualitatively show that a toxin in solution has been detected and bound by the derivatized beads.

Example 4
Detection using Heterogeneous Mixtures of Bead Particles

Two types of bead particles were made according to Example 2. Referring now to Figure 6, the colloids are of the following composition: the beads denoted by the (-) symbol are red in the images and are nonporous, silica microspheres of 6.8μm diameter covered in a fluid lipid bilayer membrane (composition: 98%DMOPC, 1% DOEPC, 1% Texas Red® DPPE). The beads denoted by the (+) symbol are white in the images and are nonporous, silica microspheres of 6.8μm diameter covered in a fluid lipid bilayer membrane (composition: 98%DMOPC, 2%DOEPC, 1% 1,2-Dioleoyl-sn-Glycero-3-Phosphoethanolamine-N-(7-nitro-2-1,3-benzoxadiazol-4-yl, or NBD-PE). The ϕ symbol refers to the approximate fraction of (+) or (-) beads, as appropriate. Analysis is identical to that performed and outlined in Example 2.

Investigations of heterogenous mixtures of colloids was accomplished by mixing dilute solutions of different colloids together at desired proportions. The resulting, heterogeneous colloid solution was then vortexed thoroughly and pipetted into a well of a 96 well plate to cast the colloid, as described above.

The analysis is performed using the equations described on page 22 of this application, entitled Hetero-bead g(r) which is hereby incorporated by reference.

For the binary colloid of Fig. 6, $\phi = 0.2$ for the entire system of heterogeneous beads. The plots on the right hand side of Fig. 6 show that the $g(r)$ plot and the first detection peak changes as the proportion of each type of bead changes.

Example 5
Detection using Bead Particles

Realistic detection experiments were performed by mixing FCS (0.1%) and cholera toxin (CTB) (at a 100nM concentration) in a sample of river water containing approximately 4mg/mL of organic and inorganic components. The mixture was filtered with a 0.2μm filter and incubated with 1mL of the bead solution for 50 minutes in the dark at room temperature, continuously mixing gently. Excess soluble components were removed by rinsing the mixture with18.2 MW-cm water prior to casting the colloid.

Upon analysis using the method of statistical analysis in Example 2, a positive signal from the system for detection of cholera was observed.

An alternative method is to disperse the beads with the cholera toxin ligand into the river, allow sufficient incubation time (say ~50 minutes), collect and isolate the beads from the river water, and then perform the analysis as outlined above.

Description of the Figures

Figure 1: Membrane-derivatized bead. (a) Schematic illustration of a membrane-derivatized silica bead. FRAP experiments conducted on the lipid membrane coating the bead's surface for (b) fluid and (c) non-fluid membranes with full illumination prior to bleach (*left*), exposure pattern during bleach (*middle*), full illumination 1 min. after bleach (*right*).

Figure 2: Mobility of membrane-derivatized beads. (a) Two-dimensional Brownian trajectories of membrane-derivatized beads, which have settled gravitationally to the bottom of a dish filled with water. (b) Time sequence images of a condensed phase of the colloid illustrating the mobility of individual beads into and out of condensed crystallites.

Figure 3: Protein binding-triggered colloidal phase transition. (a) Time sequence of images depicting the transition from a condensed to a dispersed colloidal phase, triggered by addition of protein Transitions were triggered only when the appropriate ligand was also incorporated into the membrane. (b) Corresponding plots of $g(r)$ for the time sequence in (a).

Figure 4: Protein binding asssays. (a) Plots of measured $g(r)$ functions for dispersions of beads (area fraction ϕ = 0.15) derivatized with fluid membranes (90% DMOPC, ~9% DMPS) containing different mole fractions (χ) of Texas Red-DPPE ligand, after incubation with 20 μg/ml anti-Texas Red rabbit monoclonal IgG antibody. (b) Plots of $g(r)$ for a series of identical dispersions of 6.8 μm diameter beads (ϕ = 0.25) derivatized with membranes containing the ganglioside G_{T1B}, which have been incubated with various concentrations of TT. Binding of TT to membrane surface G_{T1B} induces a condensed to dispersed phase transition as detected in the $g(r)$ plots as well as by direct observation of the colloid (inset images). (c) Series of experiments as in (b), except with 0.5% G_{M1} in place of G_{T1B}. Binding of CTB to the G_{M1} membrane surface induces the transition. Incubation of CTB with G_{T1B} colloids or TT with G_{M1} colloids produced no effect.

Figure 5:. In a parallel set of experiments on planar supported membranes, the effective dissociation constants for CTB-G_{M1} (Fig. 5A) and TT-G_{T1B} (Fig. 5B) binding were measured to be ~60 and ~41 nM, respectively. In Fig. 5C, derivatized colloids doped with G_{M1} and G_{T1B} gangliosides can be used to detect the presence of cholera and tetanus toxin.

Figure 6: A the beads denoted by the (-) symbol are red in the images and are nonporous, silica microspheres of 6.8μm diameter covered in a fluid lipid bilayer membrane (composition: 98%DMOPC, 1%DOEPC, 1% Texas Red® DPPE). The beads denoted by the (+) symbol are white in the images and are nonporous, silica microspheres of 6.8μm diameter covered in a fluid lipid bilayer membrane (composition: 98%DMOPC, 2%DOEPC, 1% 1,2-Dioleoyl-sn-Glycero-3-Phosphoethanolamine-N-(7-nitro-2-1,3-benzoxadiazol-4-yl, or NBD-PE). The ϕ symbol refers to the approximate fraction of (+) or (-) beads, as appropriate. Analysis is identical to that performed and outlined in Example 2.

Figure 7A: A schematic showing the components for the preferred embodiment of derivatized colloids which form a two-dimensional dispersion observed by a light scattering or optical microscopy.

Figure 7B: A visual representation of the *g(r)* calculations and nearest-neighbor interactions that correspond to the different peaks in the phase transition diagram of homogeneous bead particles.

References

1. Sackmann, E. Supported membranes: Scientific and practical applications. *Science* **271**, 43-48 (1996).
2. Groves, J. T. Membrane array technology for drug discovery. *Curr. Op. Drug Disc. & Dev.* **5**, 606-612 (2002).
3. Grakoui, A. et al. The immunological synapse: A molecular machine controlling T cell activation. *Science* **285**, 221-227 (1999).
4. Fang, Y., Frutos, A. G. & Lahiri, J. Membrane Protein Microarrays. *J. Am. Chem. Soc.* **124**, 2394-2395 (2002).
5. Hoffman, T. L., Canziani, G., Jia, L., Rucker, J. & Doms, R. W. A biosensor assay for studying ligand-membrane receptor interactions: binding of antibodies and HIV-1 Env to chemokine receptors. *Proc. Natl. Acad. Sci. USA* **97**, 11215-11220 (2000).
6. Yang, T., Jung, S.-y., Mao, H. & Cremer, P. S. Fabrication of phospholipid bilayer-coated microchannels for on-chip immunoassays. *Anal. Chem.* **73**, 165-169 (2001).
7. Anderson, V. J. & Lekkerkerker, H. N. W. Insights into phase transition kinetics from colloid science. *Nature* **416**, 811-815 (2002).
8. Yethiraj, A. & Blaaderen, A. v. A colloidal model system with an interaction tuneale from hard sphere to soft and dipolar. *Nature* **421**, 513-517 (2003).
9. Ramos, L., Lubensky, T. C., Dan, N., Nelson, P. & Weitz, D. A. Surfactant-mediated two-dimensional crystalization of colloidal crystals. *Science* **286**, 2325-2328 (1999).
10. Dinsmore, A. D. et al. Colloidosomes: selectively permeable capsules composed of colloidal particles. *Science* **298**, 1006-1009 (2002).
11. Manoharan, V. N., Elsesser, M. T. & Pine, D. J. Dense packing and symmetry in small clusters of microspheres. *Science* **301**, 483-487 (2003).
12. Yang, P. et al. Hierarchically ordered oxides. *Science* **282**, 2244-2246 (1998).
13. Bayerl, T. M. & Bloom, M. Physical properties of single phospholipid bilayers adsorbed to micro glass beads. *Biophys. J.* **58**, 357-362 (1990).
14. Buranda, T. et al. Biomimetic molecular assemblies on glass and mesoporous silica microbeads for biotechnology. *Langmuir* **19**, 1654-1663 (2003).
15. Wong, A. P. & Groves, J. T. Molecular topography imaging by intermembrane fluorescence resonance energy transfer. *Proc. Natl. Acad. Sci. USA* **99**, 14147 (2002).
16. Discher, D. E. & Eisenberg, A. Ploymer vesicles. *Science* **297**, 967-973 (2002).

Hetero-bead g(r)

Let's start with evaluation of $n(r)$, the actual relative density of bead pairs with separation distance r, for the four 'hetero-bead' cases:

1. n(r) of all beads

$$n_{ALL}(r) = \frac{2\eta_{ALL}(r)}{(N_R + N_W)(N_R + N_W - 1)\delta r}$$

$\eta_{ALL}(r)$ is the number of all bead pairs with separation distance $r \pm \frac{\delta r}{2}$, and N_R and N_W are total numbers of red and white beads, respectively. Since $N_R + N_W = N$ here, $n_{ALL}(r)$ is analogous to the original 'homo-bead' $n(r)$.

2. n(r) of red beads

$$n_R(r) = \frac{2\eta_R(r)}{N_R(N_R - 1)\delta r}$$

$\eta_R(r)$ is the number of red-red bead pairs with separation distance $r \pm \frac{\delta r}{2}$. If we forget about white beads, which we can do here, $N_R = N$ and $n_R(r)$ is again analogous to the original 'homo-bead' $n(r)$.

3. n(r) of white beads

With the substitution $R \to W$, $n_W(r)$ is analogous to $n_R(r)$ above.

4. n(r) of red beads against white beads

$$n_{RW}(r) = \frac{\eta_{RW}(r)}{N_R N_W \delta r}$$

$\eta_{RW}(r)$ is the number of bead hetero-pairs with separation distance $r \pm \frac{\delta r}{2}$. This $n_{RW}(r)$ formula is the only one that really differs from the 'homo-bead' $n(r)$ formula.

g(r) for the four cases

Let's use our original general definition formula:

$$g(r) = \frac{n(r)}{p(r)},$$

where $p(r)$ is the probability density of finding a bead pair with separation distance r. While $n(r)$ differed in the four discussed 'hetero-bead' cases, $p(r)$ remains unchanged from the original 'homo-bead' $p(r)$ and is:

$$p(r) = \frac{2}{X^2Y^2}\left[\pi XYr - 2(X+Y)r^2 + r^3\right].$$

Combining the formulas above, we get the following:

$$g_{ALL}(r) = \frac{\eta_{ALL}(r)X^2Y^2}{(N_R + N_W)(N_R + N_W - 1)\delta r[\pi XYr - 2(X+Y)r^2 + r^3]}$$

$$g_R(r) = \frac{\eta_R(r)X^2Y^2}{N_R(N_R - 1)\delta r[\pi XYr - 2(X+Y)r^2 + r^3]}$$

$$g_W(r) = \frac{\eta_W(r)X^2Y^2}{N_W(N_W - 1)\delta r[\pi XYr - 2(X+Y)r^2 + r^3]}$$

$$g_{RW}(r) = \frac{\eta_{RW}(r)X^2Y^2}{2N_RN_W\delta r[\pi XYr - 2(X+Y)r^2 + r^3]}$$

Since $p(r)$ is the same in all cases, the relationship between these four $g(r)$ functions comes directly from comparison of their respective $n(r)$ parts.

PROPOSED CLAIMS

1. A method of detection of an analyte in a sample,comprising the steps of:

a. providing bead particles in a well (i.e. a two-dimensionally confined area), wherein said bead particles have a ligand specific for an analyte, and allowing said beads to settle at the bottom of said well;

b. taking an image of the beads in a confined area of said well and determining the position of the center of each bead in each image to calculate pairwise the separation distance between the centers of each bead in each of said images;

c. generating a plot which maps the actual relative density of bead pairs at each separation distance divided by the probability density of finding a bead pair at each separation distance in the confined area of the well (i.e. determining if the beads are in condensed or dispersed phase);

d. adding a sample containing an analyte to be detected to said solution;

e. repeating steps b and c and comparing the plots generated by step c and step d.

2. The method of detection of claim 1, wherein the binding event between said bead particle ligand and said analyte achieves a phase transition at or near equilibrium to produce a recognizable signature effect on the random distribution of the bead particles that can be interpreted by step c of claim 1.

3. The method of claim 2, wherein the amount of bead particles provided is sufficient to produce an area fraction in the confined area of the well of 0.15 to 0.45, or more preferably from 0.15 to 0.25, wherein the area fraction is the percentage of the area in the image occupied by beads as opposed to spaces between or around beads.

4. The method of detection of claim 3, wherein said bead particles are formed from porous and nonporous forms of materials from the group consisting of silica and silica-containing compounds, polymers such as polystyrene, polymethacrylates, polyacrylates, diacetylenes, alkenes, thiophenes, polythiophenes, glycopolythiophenes, imides, acrylamides, acrylates, methacrylamides, methacrylates, vinylether, malic anhydride, urethanes, allylamines, siloxanes, anilines, pyrroles, and vinylpyridinium and other hydrogel polymeric materials, microgels and hydrogels, gold or other metals, Group II-VI

materials, Group III-V materials, branched and unbranched compositions, other inorganic and organic metals and materials acetylenes.

5. The method of detection of claim 4, wherein said bead particles are derivatized with an outer doped or undoped lipid membrane layer or derivatized with a ligand specific for an analyte.

6. The method of detection of claim 5, wherein said lipid membrane layer is comprised of lipids, cholesterols, steroids, ergosterols, polyethylene glycols, proteins, peptides, or any other molecules such as fatty acids, triacylglycerols, glycerophospholipids, sphingolipids (e.g. sphingomyelins, cerebrosides and gangliosides), sterols, cholesterol, surfactants, polysorbate, octoxynol, sodium dodecyl sulfate, zwitterionic detergents, decylglucoside, deoxycholate, diacetylene derivatives, phosphatidylserine, phosphotidylinositol, phosphatidylethanolamine, phosphatidylcholine, phosphatidylglycerol, phosphatidic acid, phosphatidylmethanol, cardiolipin, ceramide, lysophosphatidylcholine, D-erythrosphingosine, sphingomyelin, dodecyl phosphocholine, N-biotinyl phosphatidylethanolamine, and other synthetic or natural components of cell membranes that can be associated with a membrane or membrane assemblies such as liposomes and films.

7. The method of detection of claim 6, wherein said lipid membrane layer consisting essentially of a lipid selected from the group consisting of phosphatidylserine, dipalmitoylphosphatidic acid, 1,2-Dimyristoleoyl-*sn*-glycero-3-phosphocholine(DMOPC), 1,2-dimyristoyl-*sn*-glycero-3-[phospho-L-serine] (sodium salt) (DMPS), and 1,2-dioleoyl-*sn*-glycero-3-ethylphosphocholine (DOEPC), distearoylphosphatidylglycerol, phosphatidylinositol, 1,2-dioleoyl-3-dimethylammonium-propane, 1,2-dioleoyl-3-trimethylammonium–propane, dimethyldioctadecylammonium bromide, 1,2-dioleoyl-*sn*-glycero-3-ethylphosphocholine, N-(7-nitrobenz-2-oxa-1,3-diazol-4-yl)-1,2-dihexadecanoyl-*sn*-glycero-3-phosphoethanolamine ammonium salt, and and N-1,2-dihexadecanoyl-*sn*-glycero-3-phosphoethanolmine triethylammonium salt, L-a-Phosphatidylcholine (Egg PC), Cholesterol, N-Dinitrophenylaminocaproyl Phosphatidylethanolamine (DNP-Cap PE), ceramides (natural and synthetic preparations), N-[12-[(7-nitro-2-1,3-benzoxadiazol-4-yl)amino]dodecanoyl]-Sphingosine-1-Phosphocholine (C12-NBD Sphingomyelin), 1,2-

Dioleoyl-sn-Glycero-3-Phosphoethanolamine-N-(Cap Biotinyl), 1-Palmitoyl(D31)-2-Oleoyl-*sn*-Glycero-3-Phosphoinositol (and other Phosphoinositol extracts), and polyethylene glycols of various lengths.

8. The method of detection of claim 7, wherein said lipid membrane is doped with 10^{-2} to 10^{-6} M concentrations of a protein or membrane-associated ligand.

9. The method of detection of claim 1 and 8, wherein said ligand is selected from the group consisting of carbohydrates, nucleic acids, biotin, streptavidin, peptides, proteins, lipoproteins, glycoproteins, enzymes, receptors, channels, antibodies, drugs, chromophores, antigens, chelating compounds, molecular recognition complexes, ionic groups, polymerizable groups, dinitrophenols, linker groups, electron donor or acceptor groups, hydrophobic groups, hydrophilic groups, or any organic molecules that bind to receptors.

10. The method of detection of claim 9, wherein said bead particles are between 10nm and 50μm in diameter, more preferably between 1-10μm, and most preferably between about 5-6.8μm in diameter.

11. A kit for determining the presence of an analyte, comprising;

a. a well for holding beads;

b. beads coated with a fluid lipid membrane with a protein ligand embedded therein, said beads being in the well in a suspension near a transition point between condensed and dispersed phase.

Architecture and Function of Membrane Proteins in Planar Supported Bilayers: A Study with Photosynthetic Reaction Centers†

Joshua Salafsky, Jay T. Groves, and Steven G. Boxer*

Department of Chemistry, Stanford University, Stanford, California 94305-5080

Received June 17, 1996; Revised Manuscript Received August 27, 1996®

ABSTRACT: We present a simple and convenient method for creating fluid supported bilayers which contain oriented and functional photosynthetic reaction centers (RCs).[1] The supported bilayers are prepared by fusion of proteoliposomes with a glass surface. The proteoliposomes are prepared by spontaneous insertion of RCs into preformed small, unilamellar vesicles. The RCs in these vesicles are shown to be oriented with the cytochrome *c* binding surface on the outside and the H-subunit facing inside. Upon fusion to glass surfaces, the RCs remain functional and highly oriented, with the cytochrome *c* binding surface exposed to the bulk solution. The RCs in the supported bilayers are at a surface density of order 10^{11} RCs/cm^2. The quality of the supported lipid bilayer is characterized by epifluorescence microscopy and the long-range lateral mobility of the lipids by fluorescence recovery after photobleaching. We demonstrate that homogeneous, fluid bilayers can be prepared over large areas (e.g., 1 cm^2) of clean glass surfaces. The lipids in these supported bilayers are laterally mobile, and their diffusion coefficient agrees with values obtained in other fluid bilayer systems. This fluidity is unaffected by the presence of RCs; however, the RCs bearing a site-specific fluorescent label are immobile, despite retaining their charge separation and cytochrome *c* binding properties. We speculate that this results from interactions between the globular domain of the H-subunit and the glass substrate. Because of the unique spectroscopic and functional signatures associated with intact RCs, this system is one of the best characterized examples of a transmembrane protein in a supported bilayer at a nonbiological interface.

Transmembrane proteins in their native state are always uniquely oriented, and their orientation is an essential feature of their function. There are many classes of experiments which require oriented membrane proteins in a simpler lipid bilayer. Although it is often possible to insert membrane proteins into lipid vesicles with a specific orientation, the proteins are not oriented with respect to an external axis because the vesicles are freely diffusing in solution and are spherical. In order to achieve the desired polar or uniaxial orientation, it is necessary to planarize the bilayer and support it in some fashion. Three general approaches have been taken to this problem, and each has been used to study photosynthetic reaction centers (RCs):[1] the Langmuir−Blodgett (LB) technique to prepare monolayers at the air−water interface and build up single or multiple bilayer-type structures (Alegria & Dutton, 1991a,b); the black lipid membrane technique to suspend a single bilayer patch in a small aperture separating two compartments (Gopher et al., 1985); and the "piggyback" approach, in which the membrane protein of interest is bound to a second protein which is itself covalently or electrostatically bound to a surface (Amador et al., 1993). We demonstrate here a fourth technique in which supported bilayers are prepared from proteoliposome vesicles which contain oriented protein. We were motivated in developing this by an interest in preparing uniaxially oriented RCs for nonlinear optical and Stark effect measurements, as a strategy for preorganizing RCs for covalent attachment to glass or electrode surfaces, and as part of a larger program aimed at structurally characterizing and reorganizing biological membranes using applied electric fields (Groves & Boxer, 1995). In the following we describe detailed methods of preparation and characterization of both the lipid and RC protein in supported bilayers which should be applicable to other proteins as well.

The fusion of proteoliposome vesicles with a glass surface to create a planar-supported membrane was first demonstrated by Brian and McConnell (1984). In that work, the H-2K^k protein was reconstituted into egg phosphatidylcholine−cholesterol vesicles by detergent dialysis, and these were used to create a planar membrane on glass. The H-2K^k-containing membrane is useful as a model surface and is capable of eliciting a specific cytotoxic response when brought into contact with a cell. Following that work, Chan et al. (1991) demonstrated that a glycanphosphatidylinositol (GPI) anchored membrane receptor is laterally mobile in planar membranes formed from proteoliposome fusion, and this mobility enhances cell adhesion to the membrane. Other investigators have elaborated on this work by using a combination of vesicle fusion, Langmuir−Blodgett methodology, and derivatized surfaces to prepare supported

† This work was supported in part by a grant from the National Science Foundation Biophysics Program and Grant GM27738 from the National Institutes of Health.

® Abstract published in *Advance ACS Abstracts,* October 15, 1996.

[1] Abbreviations: RC, reaction center; SUV, small unilamellar vesicle; cyt *c*, cytochrome *c*; LDAO, *N,N*-dimethyldodecylamine *N*-oxide; LB, Langmuir−Blodgett; DMSO, dimethyl sulfoxide; NBD-PE, *N*-(7-nitrobenz-2-oxa-1,3-diazol-4-yl)-1,2-dihexadecanoyl-*sn*-glycero-3-phosphoethanolamine, triethylammonium salt; TCEP, tris(carboxyethyl)-phosphine; R-492, rhodamine X iodoacetamide; HABA, 4-hydroxyazobenzene-2′-carboxylic acid; Texas Red DHPE and Texas red, *N*-(Texas Red sulfonyl)-1,2-dihexadecanoyl-*sn*-glycero-3-phosphoethanolamine, triethylammonium salt; OD, optical density; bR, bacteriorhodopsin; GPI, glycanphosphatidylinositol.

S0006-2960(96)01432-8 CCC: $12.00

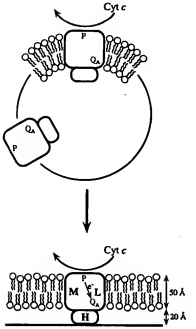

FIGURE 1: Schematic diagram of the bacterial photosynthetic reaction center in a bilayer membrane. The three protein subunits (L, M, and H) and the relevant functional components, the special pair primary electron donor, P, and the primary quinone acceptor, Q_A, are indicated. The RC is depicted in an orientation that is consistent with the results presented and a mechanism in which the vesicles fuse to the glass support by opening out.

membranes (Sui et al., 1988; Plant et al., 1995; Sackmann, 1996), though most of this work does not involve membranes which contain protein.

The RC is the smallest isolatable unit which performs the initial photoinduced charge separation steps in photosynthesis. The three-dimensional structures of RCs from two species of photosynthetic bacteria are known to atomic resolution (Deisenhofer et al., 1995). It is comprised of three subunits, termed L, M, and H, whose total molecular mass is approximately 100 kDa (see Figure 1). Its physiological role is to transduce light energy into a charge separation across the native membrane, which in turn leads to a transmembrane electrochemical potential used by the organism to store energy. The RC accomplishes this charge separation by transferring an electron from the excited state of the special pair primary electron donor, denoted P, to a quinone acceptor, denoted Q_A, to create the internal charge-separated state, $P^+Q_A^-$. The oxidized donor is subsequently reduced by a soluble ferrous cytochrome *c* (cyt *c*) which interacts with the RC at a binding site on the P face of the RC. The sidedness of this cyt *c* reduction step has been widely used to monitor the orientation of RCs in bilayer systems (Pachence et al., 1979; Venturoli et al., 1990). One of the ideal features of the RC is that the kinetics and quantum yield of formation of charge-separated species and the $P^+Q_A^-$ decay kinetics can be sensitively monitored optically, providing a built-in assay for native function. Deletion strains and plasmids for RCs from several species are available (Bylina & Youvan, 1988), so that the RC can be engineered to introduce unique functionality for labeling (Boxer et al., 1992).

EXPERIMENTAL PROCEDURES

Materials. The dye−lipid probes *N*-(Texas Red sulfonyl)-1,2-dihexadecanoyl-*sn*-glycero-3-phosphoethanolamine, triethylammonium salt (Texas Red), and *N*-(7-nitrobenz-2-oxa-1,3-diazol-4-yl)-1,2-dihexadecanoyl-*sn*-glycero-3-phosphoethanolamine, triethylammonium salt (NBD-PE), were purchased from Molecular Probes, Inc. (Eugene, OR). The thiol reductant, tris(carboxyethyl)phosphine (TCEP), and the RC conjugate, rhodamine X iodoacetamide (R-492), were also purchased from Molecular Probes. Iodoacetyl-LC−biotin, 4-hydroxyazobenzene-2′-carboxylic acid (HABA), and avidin (Immunopure avidin) were purchased from Pierce Chemical Co. Horse heart cyt *c* was purchased from Sigma Chemical Co.

Reaction Centers. RCs were isolated from *Rhodobacter sphaeroides* wild-type or the R-26 (carotenoidless) strain by methods that are described in detail elsewhere (Debus et al., 1986). The RCs isolated by this procedure generally contain only the primary quinone, Q_A. *Rb. sphaeroides* RCs have five cysteine residues at positions L92, L108, L247, H156, and H234. From an examination of the crystal structure, the cysteine residue at H156 is on the surface of the protein and the other four are buried (i.e., they are more than 10 Å from the surface). *Rhodobacter capsulatus* RCs were isolated as described in Taguchi et al. (1992). These RCs have cysteine residues at positions L92, L98, L108, L246, and L247, all of which are buried assuming the RCs have the same three-dimensional structure as the highly homologous *Rb. sphaeroides* RCs (Komiya et al., 1987). A unique surface cysteine residue was introduced on the P-face of the *Rb. capsulatus* RC by replacing the leucine residue at position M189 to create the strain (M)L189C as described in detail in Boxer et al. (1992).

RC−Biotin and RC−Rhodamine Conjugates of Rb. sphaeroides RCs. The surface of *Rb. sphaeroides* RCs can be modified using reagents which react with free cysteine groups; this was used to create RC−biotin and RC−rhodamine conjugates at the unique surface-accessible cysteine H156 (Debus et al., 1986). *Rb. sphaeroides* R-26 RCs in 10 mM Tris, pH 8.0, and 0.05% LDAO were concentrated to about 75 μM using a Centricon-30 concentrator (Amicon Co.). The RCs were then dialyzed against 10 mM Tris, pH 9.0, and 0.025% LDAO buffer for 1 day, followed by two changes of buffer containing 0.001% LDAO for 1 day each. A 10-fold molar excess of the reductant, TCEP, was added to the RC solution, and the mixture was stirred in a conical vial under nitrogen for 30 min. The conjugate, either iodoacetyl-LC−biotin or the fluorescent dye R-492, dissolved in DMSO, was then added to the mixture through a septum over a 1-min period, to a final label:RC molar ratio of 25 and a final DMSO concentration of less than 10% by volume. The mixture was stirred for 4 h at room temperature in the dark. The excess biotin label was removed by dialyzing each for 1 day against two changes of 10 mM Tris, pH 8.0, buffer containing 0.001% LDAO; the excess dye label was removed by separating it from the RC−dye conjugate using a DEAE ion-exchange column. A control RC sample was treated identically except for the addition of the biotin reagent. The dye:RC molar ratio was determined to be 1:1 from an absorption spectrum of the dye−RC complex, using extinction coefficients of 288 000 M^{-1} cm^{-1} (800 nm) and 82 000 M^{-1} cm^{-1} (590 nm; Molecular Probes catalog) for the RC

and dye, respectively. Absorption from the RC at 590 nm (10% of the 800 nm absorption) was subtracted out for these calculations. A HABA−avidin−dye solution for determining the amount of biotin conjugated to the RCs or present in the proteoliposome samples was made as 0.25 mM HABA and 0.2 mg/mL avidin in 10 mM phosphate buffer, pH 7.2, containing 150 mM NaCl (Green, 1970).

Dye Labeling of (M)L189C Rb. capsulatus RCs. Isolated (M)L189C RCs were treated with a 100 molar excess of dithiothreitol at room temperature for 15 min and then concentrated at least twice to deadstop volume in a Centricon to remove the reductant. The protein concentration was adjusted to an OD of 1−2 at 800 nm (3.5−7 μM), and the RCs were incubated for 2 h at room temperature with a 10-fold molar excess of the dye R-492 dissolved in DMSO (the final DMSO concentration was less than 10% by volume). The sample was loaded onto the column and washed with 10 mM Tris, pH 8.0, and 0.1% LDAO to elute the free dye, followed by a salt gradient, with the RC−dye complex eluting at about 300 mM NaCl. This is a higher salt concentration than is required for unmodified RCs, as expected on the basis of the added charge from the attached dye. The dye:RC molar ratio was determined to be 1:1 from the absorption spectrum and extinction coefficients given above.

Preparation of Phospholipid Vesicles. Small unilamellar vesicles (SUVs) were prepared by following the protocol outlined in Barenholz et al. (1977) using egg phosphatidylcholine (Sigma). The phosphatidylcholine was mixed with 1 mol % Texas red DHPE in HPLC-grade chloroform (Sigma-Aldrich) and dried in a vacuum desiccator overnight. The dried lipids were resuspended in 10 mM Tris, pH 8.0, buffer containing 100 mM NaCl (hereafter referred to as the standard buffer), filtered through Rainin nylon-66 0.45 μm filters using a Sibata filter unit to about 20 mg/mL, and sonicated to clarity with a Branson ultrasonicator under flowing Ar on ice for 3 min periods separated by 1 min cooling periods. The sample was then spun for 30 min at 100000*g* to remove Ti particles from the sonicator tip, and the supernatant was spun for 4 h at 166000*g* to obtain the SUVs. The SUVs were stored at 4 °C under N_2 or Ar in the dark and were used within 3 weeks. The lipid concentration in these samples was determined from the Texas Red probe absorption at 590 nm (= 100 000 M^{-1} cm^{-1}; Molecular Probes catalog, 1994), assuming that the probe concentration in the vesicles is 1 mol % as prepared. Yields (milligrams of SUV lipid per milligram of initial lipid) were calculated from this concentration and are equal to those reported by Barenholz et al. (1977).

Preparation of Proteoliposomes. Proteoliposomes were prepared according to the protocol developed by Sadler et al. (1984). RCs were concentrated to 6−11 OD (800 nm) in 10 mM Tris, pH 8.0, and 0.1% LDAO buffer using a DEAE ion-exchange column or Centricon concentrator, and the salt concentration was adjusted to 100 mM NaCl by dialysis. The RCs were added to the SUVs in a small conical-bottom vial with stirring, typically to a final RC:lipid mole ratio of 1:350. Samples were then run down a Sepharose CL-4B (Sigma Co.) column, previously equilibrated with SUVs to minimize lipid adsorption, and fractions were collected. The absorption spectra of the proteoliposome fractions were measured, and the RC:lipid mole ratio was calculated using the absorption peak of the Texas red lipid label. Typically, the mole ratio of RC:lipid in the fractions follows a monotonic decrease, beginning at about 1:300 and ending with 1:1000−1200. Only the fractions with a mole ratio of about 1:500 or lower are used to make planar-supported bilayers; the fractions with higher mole ratios do not always form uniform planar bilayers.

Cytochrome c Trapping in SUVs and Proteoliposomes. Horse heart cytochrome *c* was trapped inside SUVs by sonicating the lipids in the presence of 8 mM cyt *c*. The cyt *c* was prereduced with sodium dithionite, and the reductant was removed with a Sephadex G-50 (Sigma) filtration column. Cyt *c* external to the SUVs was separated from the SUVs with trapped cyt *c* on a Sepharose CL-4B column previously equilibrated with SUVs to minimize lipid adsorption. No further change in the cyt *c* content was observed upon running these SUVs down a second CL-4B column, demonstrating that the cyt *c* is stably trapped inside. Proteoliposomes with trapped cyt *c* were prepared by using these SUVs with trapped cyt *c*. A control was performed to demonstrate that added cyt *c* could be separated from proteoliposomes on a CL-4B column.

Function and Orientation of RCs in Proteoliposomes: P^+Q^- Recombination Kinetics. The $P^+Q_A^-$ recombination kinetics in RCs were measured at room temperature by exciting the samples with a saturating 10 ns 532 nm YAG laser pulse gated at 2 Hz. The change in absorption was probed at 865 nm using light from a 100 W tungsten bulb, powered by a 12 V regulated supply (Model PAL16−20, Kikusui Co., Yokohama, Japan), passed through a single monochromator with a resultant bandwidth of about 1 nm. The probe light intensity at the sample was 10 μW/cm^2. The change in absorption was detected with a home-built detector using an HUV-1100BG photodiode (EG&G Co.) with a measured response time of 1 ms (adequate for the 100 ms $P^+Q_A^-$ decay while minimizing higher frequency noise).

The orientation of the RCs was measured by observing whether ferrous cyt *c* reduces P^+ as outlined in Pachence et al. (1977). The relevant reaction scheme and kinetics are

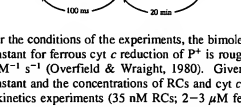

Under the conditions of the experiments, the bimolecular rate constant for ferrous cyt *c* reduction of P^+ is roughly 1 10^7 M^{-1} s^{-1} (Overfield & Wraight, 1980). Given this rate constant and the concentrations of RCs and cyt *c* used in our kinetics experiments (35 nM RCs; 2−3 μM ferrous cyt *c*), virtually all of the RCs with accessible P-faces in the proteoliposomes will be reduced by the cyt *c* within 15 ms. By probing the amplitude of the P^+ decay with and without cyt *c*, the accessibility of the P-face can be determined.

Preparation and Characterization of Planar Supported Bilayers Containing RCs. The planar bilayers were formed by exposing a clean glass coverslip (Corning cover glass, 18 mm square; cleaned by rinsing with distilled water and then baking at 450 °C for 5−8 h) to a sample of the proteoliposomes (lipid concentration 0.1 mg/mL or higher) for 5−10 min. The resulting supported bilayer must be kept hydrated at all times and was destroyed if exposed to air.

Three methods were used for making the supported bilayers: (i) For fluorescence microscopy studies, the supported bilayer was made on one side only by dropping the coverslip onto a 100 μL drop of proteoliposome solution in a clean petri dish. After incubating, the excess proteoliposome solution was washed away with the standard buffer, and the coverslip was transferred under the same buffer to a microscope slide with the supported bilayer side facing into the well to keep the bilayer hydrated. (ii) For absorption spectroscopy, both sides of the square coverslip were coated with supported bilayer by immersion in a Teflon trough with 1 mm wide slits cut to a depth of half the height of the coverslip. This produces supported bilayer on both sides of a coverslip, but only half-coated on each side. Eleven glass coverslips were placed into a slotted Teflon holder with 1 mm between each surface and immersed in the standard buffer in a 30 mm square cuvette (Wilmad Glass Co.). An absorption baseline was obtained by scanning the uncoated portion against air with a spectral slit width of 2 nm, at a scan rate of 960 nm/min. The cuvette was then carefully translated in the spectrometer compartment to the supported bilayer side of the coverslips; this side was scanned as the sample. Averages were made by averaging separately made scans. (iii) For $P^+Q_A^-$ recombination kinetics measurements, the coverslips were fully coated with supported bilayer by complete immersion in a Teflon trough.

The $P^+Q_A^-$ recombination kinetics of RCs in supported bilayers were measured using the same setup described above for the proteoliposomes, except the probe light was detected with a home-built two-stage capacitively coupled detector (Joe Rolfe, Stanford University electronics shop). Eleven glass coverslips, fully coated on both sides with bilayer, were placed into the Teflon holder in the 30 mm^2 cuvette and were excited at an angle of about 20° to the probe beam. Prereduced cyt *c* was added by immersing the square cuvette in a bath containing a solution of this protein.

The uniformity and fluidity of the supported bilayers were monitored by epifluorescence microscopy (Nikon Labophot microscope with rhodamine and fluorescein filters) using either the fluorescent dye−lipid probe or fluorescently labeled RCs. Observations of the bilayer were made with the 10 or 40 objectives giving essentially diffraction-limited resolution of the membrane. Photographs of bilayer fluorescence were taken with a Nikon F3 camera mounted on the microscope. Photobleaching of the bilayer was accomplished by illuminating a portion of the membrane continuously with the excitation light; a circular region was bleached by shadowing with the microscope aperture.

Moles of Lipid in Supported Bilayers Containing RCs. The lipid content of the supported membranes was determined by quantitative fluorescence measurements of the resolubilized films. Membranes were dissolved off the surface into a known volume of the standard buffer with 0.1% LDAO for fluorescence measurements. Standard solutions were made by dissolving known amounts of the same lipid mixture used to make SUVs into the 0.1% LDAO buffer. The fluorescence intensity at 610 nm of the dye−lipid probe in this solution was measured with a fluorometer and calibrated against that of a standard using a square 1 cm path-length cuvette in front-face collection mode. These measurements confirm that vesicle fusion consistently produces single supported bilayers.

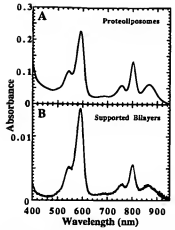

FIGURE 2: (A) Absorption spectrum of RC-containing proteoliposomes in the standard buffer at room temperature. The lipid contains 1 mol % Texas Red DHPE whose absorption maximum occurs at 590 nm and from which the RC:lipid ratio can be obtained (1:500 for the case shown). Comparing the magnitude of this peak with the 800 nm peak of the RC allows calculation of the RC:lipid ratio. The distinctive set of three absorption peaks from 700 to 900 nm is due to bacteriochlorophyll and bacteriopheophytin cofactors in the RC and is sensitive to the structural integrity of the RC complex. (B) Absorption spectrum of 11 glass coverslips, each coated on both sides with supported lipid bilayers containing RCs, measured at room temperature in the standard buffer (average of two scans). The magnitude of the RC absorption indicates an RC surface density on the order of 10^{11} RCs/cm^2 and a surface coverage of 10%; the magnitude of the absorption peak at 590 nm due to the Texas Red DHPE dye−lipid probe is consistent with a single bilayer architecture.

RESULTS

Absorption Spectrum of Proteoliposomes. A typical absorption spectrum of the proteoliposomes is shown in Figure 2A. The ratio of the absorption of the dye-labeled lipid to the RCs is used to calculate the molar ratio between the lipids and the RC. Ratios vary with proteoliposome fraction from 1:350 to 1:1200 (the sample shown is 1:500). At this mole ratio, the surface area coverage of the RCs in the vesicle bilayer is about 10%, assuming an area of 70 Å^2 occupied by a lipid molecule (Gennis, 1989) and 2500 Å^2 (Yeates et al., 1987) occupied by the RC.

Absorption Spectrum of RCs in Supported RC Bilayers. The absorption spectrum of RCs in supported lipid bilayers on glass was measured to provide four important pieces of information. First, the line shape demonstrates that the RCs are structurally intact in the supported bilayers as shown in Figure 2B. Second, the magnitude of the RC absorption indicates the RC coverage is of the order of 10^{11} RCs/cm^2. For most samples, the RC:lipid mole ratio is 1:550, which corresponds to an RC surface coverage of 10%. Third, the magnitude of the dye−lipid absorption indicates a single lipid bilayer. The single bilayer nature of the supported membranes is further confirmed by quantitative fluorescence of the resolubilized membranes. Fourth, the mole ratio of RCs to lipid in the supported bilayers is approximately equal to that of the proteoliposomes used to make them; the agreement is more exact when more homogeneous proteoliposome fractions are deposited. This indicates that the glass-supported structure is a single bilayer formed from the vesicle bilayer and that the RCs remain associated with the bilayer during the fusion process.

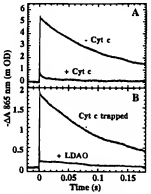

FIGURE 3: (A) $P^+Q_A^-$ recombination kinetics of RCs in proteoliposomes without and with addition of ferrous cytochrome *c* in the standard buffer measured at room temperature. The concentrations of RCs and cyt *c* are 35 nM and 2 μM, respectively. The traces are an average of 700 shots. The data demonstrate that the protein is functional and oriented in proteoliposomes with the P-side facing outward. (B) $P^+Q_A^-$ recombination kinetics of RCs in proteoliposomes with ferrous cytochrome *c* trapped inside and upon disruption of the proteoliposomes by addition of 0.01% LDAO in the standard buffer at room temperature. The concentrations of RCs and cyt *c* are 27 and 200 nM, respectively. The traces are an average of 700 shots. The data demonstrate that the lipid structures are vesicular and that trapped cyt *c* cannot access the P-face (cyt *c* binding site) of the RCs in proteoliposomes.

Function and Orientation of RCs in Proteoliposomes. Three experiments are presented to demonstrate that the RCs are embedded in the vesicle lipid bilayer and are oriented with the P-face out and the Q-face (H-subunit) facing inward as illustrated in Figure 1. One experiment demonstrates that the P-face of the RCs in proteoliposomes is accessible to the external solution; a second experiment demonstrates that the vesicles are capable of trapping cyt *c* and that the RC P-face is not accessible to the trapped cyt *c*; a third experiment shows that the H-subunit is not accessible to the external solution using a specific and unique biotin label.

First, the percentage of RCs with accessible cyt *c* binding sites was determined using the bleach amplitudes of $P^+Q_A^-$ recombination kinetics with and without added cyt *c*, as described by Pachence et al. (1979). Briefly, this is determined from the ratio of the bleach amplitude with added cyt *c* to the bleach amplitude without cyt *c* following excitation with a saturating flash. A single flash was used to measure the rate of reduction of the bleach amplitude of P^+ by cyt *c* to determine that all of the bleach amplitude is eliminated by cyt *c* within 20 ms, as expected given the known rate constant and reactant concentrations (Overfield & Wraight, 1980). Multiple flash data were then taken and the bleach amplitudes were used to determine the accessibility of the P-face of the RCs in the proteoliposomes. The results of these experiments are shown in Figure 3A. The data were fit to a single exponential to determine a rate constant of 7.2 s^{-1} for $P^+Q_A^-$ recombination, which demonstrates that the RCs are functional in proteoliposomes (Pachence et al., 1979). From the ratio of the bleach amplitudes at 20 ms for the traces without and with added cyt *c*, the percentage of RCs in proteoliposomes with the cyt *c* binding site accessible is 95%.

Second, we demonstrate that the lipid structures are vesicular and assay for the percentage of RCs with cyt *c* binding sites exposed to the interior of the vesicles by trapping cyt *c* within SUVs and proteoliposomes. The cyt *c* is first trapped within SUVs, and these are used to make proteoliposomes. An absorption spectrum of proteoliposomes with trapped cyt *c* was measured to determine the cyt *c*:RC mole ratio, which was found to be about 6:1 using the known extinction coefficients of each (data not shown). This and the observation that vesicles could be passed through a sizing column without loss of trapped cyt *c* demonstrate that stable vesicular structures are present. The $P^+Q_A^-$ recombination kinetics of RCs in proteoliposomes with trapped cyt *c* is shown in Figure 3B. The bleach amplitude is within 5% of that measured on an OD-matched sample of detergent-solubilized RCs in the absence of cyt *c*. This demonstrates that 95% of the cyt *c* binding face is oriented outward (binding of trapped cyt *c* to lipids could interfere with binding to RCs, but the cyt *c* exhibits negligible binding to egg phosphatidylcholine vesicles (Rytomaa et al., 1992; Gennis, 1989). Addition of LDAO (0.01%) disrupts the vesicles releasing the cyt *c* which can then bind to RCs. As shown in Figure 3B, this reduces the bleach amplitude of the recombination kinetics. The extent of the bleach amplitude reduction is determined by the number of cyt *c* molecules in the reduced state per RC.

From the results of the first two orientation experiments, the RCs are either embedded in the vesicle bilayer with the H-subunit facing inward as illustrated in Figure 1 or they are associated with the vesicles in some nonspecific way outside of them. The third experiment was designed to resolve these two alternatives as follows. A molecule of biotin was bound covalently to the unique cysteine residue at position (H)156 in *Rb. sphaeroides* RCs (Debus et al., 1986), creating a label for probing the H-subunit accessibility in proteoliposomes. The biotin is colorimetrically detected using a HABA−avidin solution as described by Pierce (Pierce Chemical Co. catalog). Briefly, the HABA dye binds to the biotin-binding sites in avidin; it has a large absorption at 500 nm in this state and a very small absorption in the free state (difference in extinction coefficient at 500 nm between the two states is 34 000 M^{-1} cm^{-1}). Added biotin (free or covalently bound to protein) will quantitatively displace the bound HABA, and the resultant decrease in absorption at 500 nm can be used to determine the amount of added biotin.

The HABA−avidin solution was placed into cuvettes in both the sample and reference paths of the spectrometer, and a baseline was measured. The biotin-labeled RCs or unlabeled control RCs were then added to the sample cuvette, and the absorption spectrum was measured as shown in Figure 4A. From the difference in absorption at 500 nm of the biotin-labeled RCs and control RCs, the biotin:RC molar ratio can be determined. The molar ratio is determined using the absorption at 800 nm (extinction coefficient of 288 000 M^{-1} cm^{-1} for the RCs) and the difference in absorption between the biotin-labeled and control RCs of the HABA dye at 500 nm (extinction coefficient difference of 34 000 M^{-1} cm^{-1}). From this analysis, the molar ratio of biotin:RC is 1:1, which is consistent with the label bound to the single, free cysteine at H-156.

Proteoliposomes were then prepared using the biotin-labeled RCs, and these were added to the HABA−avidin solution to test for the presence of biotin as shown in Figure 4B. There is no change in the absorption at 500 nm, which indicates that there is no exposed biotin in the proteoliposomes with biotin-labeled RCs, consistent with the RCs being

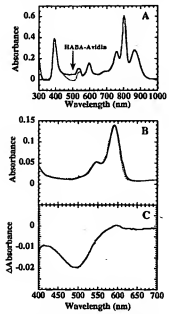

FIGURE 4: (A) Absorption spectra of biotin-labeled RCs (labeled on the H-subunit) (---) and control (unlabeled) RCs (—) added to the HABA−avidin solution. A baseline was measured with HABA−avidin solution alone. (B) Absorption spectrum of RC−biotin proteoliposomes (—) and RC proteoliposomes (---) added to the HABA−avidin solution. The spectra were normalized at 590 nm. (C) Difference absorption spectrum of biotin−RC proteoliposomes against RC proteoliposomes with trace LDAO (0.001%) added to each in HABA−avidin solution. The baseline is the absorption due to the biotin−RC and RC proteoliposomes in the HABA−avidin solution.

embedded in the vesicles with the H-subunit facing inward. A control was performed to demonstrate that RC (without biotin) proteoliposomes do not produce a signal for biotin when added to the HABA−avidin solution; this is shown in Figure 4B. Finally, the difference absorption spectrum of the biotin-labeled RCs in proteoliposomes and unlabeled RCs in proteoliposomes with trace addition of LDAO (0.001%) to disrupt the vesicles is shown in Figure 4C. There is no further change in the absorption upon addition of a second aliquot of LDAO. The signal is of the expected magnitude (using the measured concentration of RCs in these samples, a molar biotin:RC ratio of 1:1, and a difference extinction coefficient of 34 000 M^{-1} cm^{-1} for the HABA dye) and confirms that the RCs are embedded in the vesicle lipid bilayer and are oriented with the H-subunit facing the interior.

Function and Orientation of RCs in Supported RC Bilayers: P^+Q^- Recombination Kinetics. The $P^+Q_A^-$ recombination kinetics of the RCs in supported bilayers were measured to demonstrate the functionality of the RCs as shown in Figure 5.

The decay kinetics were fit to a single exponential with a rate constant of 7.9 s^{-1}, which demonstrates that the RCs are functional (Pachence et al., 1979). Addition of cytochrome *c* results in a disappearance of the bleach amplitude of the millisecond recombination kinetics, demonstrating that more than 90% of the RCs are oriented in the supported bilayer with the P-face accessible to the bulk solution. The cyt *c* was then removed by successive buffer dilution, and the bleach amplitude of the RCs was found to return to its original amplitude within 2 h. This is consistent with the time reported elsewhere (Gopher et al., 1985) for recovery

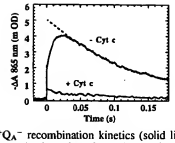

FIGURE 5: $P^+Q_A^-$ recombination kinetics (solid line) and single exponential fits to the data after 50 ms (dashed line, see text) of 11 glass cover slips with supported lipid bilayers containing RCs in the absence and upon addition of 10 μM ferrous cyt *c*. The recombination time of the kinetics in the absence of cyt *c* demonstrates that the RCs are functional in supported bilayers. Nearly complete loss of the bleach amplitude upon addition of cyt *c* indicates the RCs are oriented with the P-side (cyt *c* binding site) facing bulk solution.

of the PQ_A^- state to the PQ_A state, where reversible charge separation to produce $P^+Q_A^-$ can then occur again in the absence of cyt *c*. The supported bilayers were uniform and unchanged upon addition of the cyt *c*, as observed by fluorescence microscopy of the fluorescent dye−lipid probe. The initial sharp rise in the bleach amplitude is due to scattered excitation light into the detector, and the initial round off in the decay is due to the instrument response of the detector which truncates the initial bleach amplitude by 20%. The detector response due to the scattered excitation light decays to the preflash baseline with 50 ms; the kinetic traces were fit using data after this initial 50 ms artifact, and these fits were used to obtain the initial bleach amplitude.

Fluorescence Imaging of Lipids in Supported Bilayers Containing RCs. Visualization of supported membranes using epifluorescence microscopy was also an invaluable test of membrane quality and was used as a check for bilayer formation after each deposition. The bilayer was scratched with the tip of a pair of tweezers, which removes bilayer creating boundaries to lateral diffusion. A bilayer of high integrity appears as a fairly uniform field of fluorescence; a typical example is shown in Figure 6A. A nonuniform bilayer appears as a field of fluorescence with dark spots or patches distributed throughout the field, while failure to form bilayers appears as a field of bits of fluorescence separated by dark space between unfused vesicles, visible as brighter dots of fluorescence. Vesicles are not adsorbed to the planar membranes. Generally, the proteoliposome fractions with lower RC:lipid mole ratios (<1:700) give the most uniform planar bilayers.

The bilayer lipids are laterally mobile, as demonstrated by photobleaching a small spot of the dye−lipid using the microscope aperture and watching the fluorescence within this spot recover with time. We assume that the mobility of the dye−lipid indicates general membrane mobility. Figure 6A depicts a photobleached spot shortly after bleaching; the same region is shown after 20 min in Figure 6B. Complete fluorescence recovery after photobleaching of regions outside the enclosed triangle indicates all lipids are mobile over long distances; no immobile fraction is observed. Trapping of bleached dye−lipid within the triangle demonstrates the lateral nature of the lipid mobility; the dye−lipid is not partitioning into the bulk solution, which would result in some recovery in this region.

Crude estimates of the diffusion coefficient were obtained by observing the time scale of the recovery of a spot

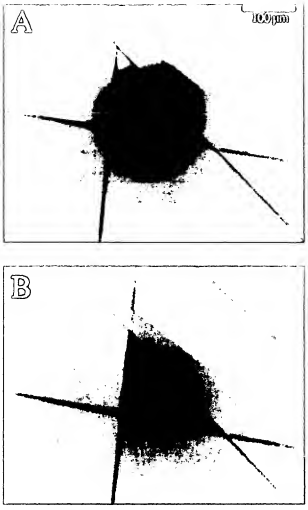

FIGURE 6: (A) Photograph of fluorescence from supported bilayers containing RCs on glass. The mole ratio of RC:lipid in the sample shown is about 1:700. One mole percent of Texas Red DHPE was used as the fluorescent lipid. The sharp dark lines are scratches in the lipid bilayer surface that create physical boundaries to lateral diffusion of the lipids. Prior to being scratched, the surface appeared homogeneous. A circular region of the lipid was shadowed out by the microscope aperture and photobleached with the excitation light. (B) The same field of view 20 min after photobleaching. The photobleached area now fills the central bounded triangular region; other unbounded regions outside the triangle have recovered a substantial amount of fluorescence, as long-range lateral diffusion of fluorescent and photobleached lipid leads to mixing. These results demonstrate that the lipid component is freely diffusing in two dimensions. The fact that bounded regions remain bleached indicates that dye−lipid partitioning into the aqueous phase and spontaneous fluorescence recovery are negligible.

unhindered by scratch boundaries. The diffusion coefficient, D, is related to the half-life of this recovery: $D = r^2/4\tau$ (Sackmann, 1980), where r is the radius of the spot and τ is the time it takes for half of the integrated fluorescence intensity to return. A spot 200 μm in diameter shows significant recovery in 5−10 min, indicating that τ is within this range giving diffusion coefficients of 4−8 $\mu m^2/s$, which is in agreement with the values found by others in more quantitative experiments [4.4 ± 0.5 $\mu m^2/s$; see Stelzle et al. (1992)].

Fluorescence Imaging of Labeled RCs in Supported Bilayers Containing RCs. Rb. sphaeroides RCs covalently labeled at cysteine (H)156 (the H-subunit side) with the cysteine-reactive fluorescent rhodamine dye R-492 were used for imaging the protein component in the supported bilayers. These supported bilayers were doped with 1 mol % of NBD-PE instead of the Texas red lipid label, due to overlap of the fluorescence spectrum of the Texas red label with that of R-492. The fluorescence intensity of the labeled RCs in supported bilayers is uniform across the surface of the glass and exactly matches the scratch patterns of the fluorescent dye−lipid probe for a given sample. Observations of the fluorescence intensity were made over a 30 min period following bleaching of a roughly 100 μm diameter spot. Unlike the lipids described above, the RCs exhibit no lateral diffusion on this time scale. Diffusion coefficients of fluid protein components in a natural membrane have values between 1 and 5 $\mu m^2/s$ (Gennis, 1989), so the labeled RCs in the supported bilayers are essentially immobile.

An identical experiment was performed with the *Rb. capsulatus* RC mutant (M)189LC, labeled with the fluorescent dye R-492. This experiment was performed to investigate whether the lack of mobility of the H-subunit labeled *Rb. sphaeroides* RCs might be due to interactions between the fluorescent label and the glass substrate (cf. Figure 1). The engineered cysteine is expected to be the only free, surface cysteine (H-156 cysteine is absent in the *Rb. capsulatus* RC) from a consideration of the crystal structure of the *Rb. sphaeroides* RC and its high sequence homology with the *Rb. capsulatus* RCs (Komiya et al., 1987); this is verified experimentally, as the resultant dye−RC conjugate has a molar ratio of dye to RC of 1:1. The position of the engineered cysteine is situated in the binding site of the cyt *c*, on the opposite side of the RC from the H-subunit. No mobility of these RCs was observed in supported bilayers.

DISCUSSION

Our goal in this work was to create an architecture with oriented RCs on a solid support. The results demonstrate that RC-containing proteoliposomes can be created from preformed SUVs in a highly asymmetric way with the cytochrome *c* binding site facing outward. This is consistent with the result reported by Sadler et al. (1984) but is further substantiated by the biotin labeling experiments which, along with the cyt *c* binding experiments, demonstrate that the RC is genuinely oriented in a trans-bilayer configuration.

The RCs remain oriented in supported bilayers with the cytochrome *c* binding site facing the bulk solution, as illustrated schematically in Figure 1. This indicates that vesicle fusion occurs in a way which opens the side of the vesicles near the glass surface, followed by a flattening of the vesicles from a spherical to a planar shape. Other evidence for this fusion mechanism can be found in the work of Contino et al. (1994). It is conceivable that one could direct the orientation of a protein in proteoliposomes and, consequently, in supported bilayers by binding charged molecules to the protein's surface or modifying it in some other way.

There is evidence that the distribution of charges on the surface of a protein determines its orientation in proteoliposomes. For example, Steverding et al. (1990) have shown that the net orientation of bovine heart cytochrome *c* oxidase can be changed from one direction to the other by chemically modifying the lysine amino groups to make them negatively charged; however, in neither case is the net

orientation greater than 40%. The issue of orientation in reconstitution has also been studied using bacteriorhodopsin (bR) as a model protein and by varying detergent type, concentration, and removal method (Rigaud et al., 1987). An important conclusion is that when bR was incorporated into preformed vesicles, it orients unidirectionally.

The observation that RCs in the supported bilayers are immobile, while the lipids are fully fluid, suggests that the protein interacts with the glass surface. In the supported membranes described here, the RCs are oriented with the H-subunit facing toward the glass surface. Packing models of a lipid bilayer around the RCs indicate that the H-subunit domain projects roughly 20 Å outside of the bilayer (Deisenhofer et al., 1984; Yeates et al., 1987), which is the approximate distance found between the membrane surface and the support for pure supported bilayers on glass (Bayerl & Bloom, 1990) and quartz (Johnson et al., 1991). The transmembrane protein H-2K^k (Brian et al., 1984) and the transmembrane isoform of LFA-3 (lymphocyte function-associated antigen 3) were also found to be immobile in supported bilayers (Chan et al., 1991). In contrast, highly mobile proteins associated with supported lipid bilayers can be made if they are tethered to the membrane by a GPI linker (Chan et al., 1991; Groves et al., 1996).

Preliminary studies using the transparent semiconductor indium−tin oxide (ITO) indicate that vesicle fusion can be used to form an organized interface between RCs and this material. Proteoliposomes spontaneously fuse with the naturally hydrophilic ITO surface to form a uniform layer as observed by epifluorescence microscopy. Quantitative fluorescence of the resolubilized film suggests that the lipid content is consistent with single bilayer coverage as for glass supports. In contrast to glass-supported bilayers, both the lipid and RC protein were immobile on ITO as seen by the failure of photobleached spots to recover fluorescence. Absorption spectra indicate that the RCs are structurally intact. Measurements of the $P^+Q_A^-$ charge recombination kinetics were compromised by absorption and scatter from the ITO film itself. Rough data confirm that the RCs are functional and at least 80% oriented with the same orientation as on glass.

The supported bilayer system made by fusion of proteoliposomes is an attractive alternative to other membrane systems. Langmuir−Blodgett (LB) techniques are highly sensitive to experimental conditions and labor intensive. Black lipid membranes (BLMs) closely resemble lipid bilayers and are well suited to electrical measurements under near physiological conditions, but they are not so easily manipulated or mechanically robust as supported bilayers. It is also difficult to control or measure the amount of protein incorporated into BLMs. Furthermore, supported bilayers can be prepared over large areas (> cm^2) unlike the BLMs (typical area of 0.01 cm^2). The RCs are also oriented unidirectionally by the SUV−proteoliposome method rather than bidirectionally with the BLM (Gopher et al., 1985). The use of self-assembled monolayers to bind detergent-solubilized proteins directly has not been reported and is likely quite sensitive to detergent−surface interactions. Derivatized surfaces which bind monolayers of cytochrome *c* to which RCs have been bound have been reported (Amador et al., 1993); however, in this case both the cytochrome *c* and RCs are adsorbed to the surface at densities significantly higher than close packed (twice and three to four times, respectively), which suggests that the protein−surface architecture is not clearly defined.

In conclusion, we have demonstrated the use of a vesicle fusion method to create planar-supported bilayers which contain oriented and fully functional RCs. The RCs were first reconstituted into proteoliposomes with unidirectional orientation by insertion into preformed SUVs. The structural integrity, functionality, and orientation of the RCs are preserved when the proteoliposomes are deposited as supported bilayers.

This work provides a uniquely well-defined picture of the supported protein−lipid bilayer architecture. The RC-containing supported membranes are stable for at least weeks, a testament to the native-like environment provided by the architecture. The results presented here, along with the convenience and generality of the vesicle fusion method, suggest that supported bilayers may be useful in a much wider range of applications.

ACKNOWLEDGMENT

We are indebted to Professors McConnell and Huestis in this Department for the generous use of their epifluorescence microscopes.

REFERENCES

Alegria, G., & Dutton, P. L. (1991a) *Biochim. Biophys. Acta 1057*, 239−257.

Alegria, G., & Dutton, P. L. (1991b) *Biochim. Biophys. Acta 1057*, 258−272.

Amador, S. M., Pachence, J. M., Fischetti, R., McCauley, J. P., Jr., Smith, A. B., III, & Blasie, J. K. (1993) *Langmuir 9*, 812−817.

Barenholz, Y., Gibbes, D., Litman, B. J., Goll, J., Thompson, T. E., & Carlson, F. D. (1977) *Biochemistry 16*, 2806−2810.

Bayerl, T. M., & Bloom, M. (1990) *Biophys. J. 58*, 357−362.

Boxer, S. G., & Woodbury, N. W. (1992) *Biochemistry 31*, 10345−10355.

Boxer, S. G., Stocker, J., Franzen, S., & Salafsky, J. (1992) *AIP Conf. Proc. 262*, 226−236.

Bylina, E. J., & Youvan, D. C. (1988) *Proc. Natl. Acad. Sci. U.S.A. 85*, 7226−7230.

Chan, P., Lawrence, M. B., Dustin, M. L., Ferguson, L. M., Golan, D. E., & Springer, T. A. (1991) *J. Cell Biol. 10*, 245−255.

Contino, P. B., Hasselbacher, C. A., Ross, J. B. A., & Nemerson, Y. (1994) *Biophys. J. 67*, 1113−1116.

Debus, R. J., Feher, G., & Okamura, M. Y. (1986) *Biochemistry 25*, 2276−2287.

Deisenhofer, J., Epp, O., Miki, K., Huber, R., & Michel, H. (1984) *J. Mol. Biol. 180*, 385−398.

Deisenhofer, J., Epp, O., Sinning, I., & Michel, H. (1995) *J. Mol. Biol. 246*, 429−457.

Gennis, R. B. (1989) in *Biomembranes* (Cantor, C. R., Ed.) Springer-Verlag, New York.

Gopher, A., Blatt, Y., Schonfeld, M., Okamura, M. Y., Feher, G., & Montal, M. (1985) *Biophys. J. 48*, 311−320.

Green, N. M. (1970) in *Methods in Enzymology*, pp 418−427, Academic Press, New York.

Groves, J. T., & Boxer, S. G. (1995) *Biophys. J. 69*, 1972−1975.

Groves, J. T., Wülfing, C., & Boxer, S. G. (1996) *Biophys. J. 71*, 2716−2723.

Johnson, S., Bayerl, T., McDermott, D., Adam, G., Rennie, A., Thomas, R., & Sackmann, E. (1991) *Biophys. J. 59*, 289−294.

Komiya, H., Yeates, T. O., Rees, D. C., Allen, J. P., & Feher, G. (1987) *Proc. Natl. Acad. Sci. U.S.A. 85*, 9012−9016.

Overfield, R. E., & Wraight, C. A. (1980) *Biochemistry 19*, 3322−3327.

Pachence, J. M., Dutton, P. L., & Blasie, J. K. (1979) *Biochim. Biophys. Acta 548*, 348−373.

Plant, A. L., Brigham-Burke, M., Petrella, E. C., & O'Shannessy, D. J. (1995) *Anal. Biochem. 226*, 342−348.

Rigaud, J., Paternostre, M., & Bluzat, A. (1988) *Biochemistry 27*, 2677−2688.

Rytomaa, M., Mustonen, P., & Kinnune, P. K. (1992) *J. Biol. Chem. 267*, 22243−22248.

Sackmann, E. (1980) in *Physical basis of trigger processes and membrane structures* (Chapman, D., Ed.) pp 105−143, Academic Press, London.

Sackmann, E. (1996) *Science 271*, 43−48.

Sadler, D. M., Rivas, E., Gulik-Krzywicki, T., & Reis-Husson, F. (1984) *Biochemistry 23*, 2704−2712.

Stelzle, M., Miehlich, R., & Sackmann, E. (1992) *Biophys. J. 63*, 1346−1354.

Sui, S.-f., Urumow, T., & Sackmann, E. (1988) *Biochemistry 27*, 7463−7469.

Taguchi, A. K. W., Stocker, J. W., Alden, R. G., Causgrove, T. P., Peloquin, J. M., Boxer, S. G., & Woodbury, N. W. (1992) *Biochemistry 31*, 10345−10355.

Venturoli, G., Melandri, B. A., Gabellini, N., & Oesterhelt, D. (1990) *Eur. J. Biochem. 189*, 105−112.

Yeates, T. O., Komiya, H., Rees, D. C., Allen, J. P., & Feher, G. (1987) *Proc. Natl. Acad. Sci. U.S.A. 84*, 6438−6442.

BI9614321

Electrical Manipulation of Glycan-Phosphatidyl Inositol-T th r d Prot ins in Planar Supported Bilay rs

Jay T. Groves,* Christoph Wülfing,# and Steven G. Boxer*
Departments of *Chemistry and #Microbiology and Immunology, Stanford University, Stanford, California 94305-5080 USA

ABSTRACT Electric fields have been used to manipulate and concentrate glycan-phosphatidyl inositol (GPI)-tethered proteins in planar supported bilayers. Naturally GPI-linked CD48, along with engineered forms of I-E^k and B7-2, in which their transmembrane domains have been genetically replaced with the GPI linkage, were studied. The proteins were labeled with fluorescently tagged antibodies, allowing the electric field-induced behavior to be followed by epifluorescence microscopy. All three protein complexes were observed to migrate toward the cathode with the B7-2 and CD48, each tethered to the membrane by a single GPI linker, moving significantly faster than the I-E^k, which has two GPI linkers. Patterns scratched int the membrane function as barriers to lateral diffusion and were used to isolate the proteins into highly concentrated corrals. All field-induced concentration profiles were completely reversible, indicating that the supported bilayer provides a stable, fluid environment in which GPI-tethered proteins can be manipulated. The ability to electrically control the spatial distribution of membrane-tethered proteins provides new opportunities for the study of biological membranes and the development of membrane-based devices.

INTRODUCTION

Unilamellar phospholipid vesicles spontaneously fuse with an appropriate hydrophilic surface to form a continuous supported bilayer (Brian and McConnell, 1984; Sackmann, 1996). The vesicle fusion process is quite general, accommodating a variety of substrates and lipid compositions as well as the incorporation of proteins (Kalb et al., 1992; Rädler et al., 1995; Salafsky et al., 1996; Watts et al., 1984). The supported membrane is separated from the solid support by a 10–20-Å film of water (Bayerl and Bloom, 1990; Johnson et al., 1991) and retains many of the properties of free membranes, including lateral fluidity. This fluidity is truly long-range, with mobile components of both leaflets of the bilayer freely diffusing over the entire surface of the support. Molecules confined to a supported bilayer are thus uniquely sensitive to electrical manipulation. Microelectrophoresis in supported bilayers has been demonstrated (Stelzle et al., 1992) and, more recently, combined with patterns of lateral diffusion barriers to generate steady-state concentration gradients of charged lipid probes in the supported membrane (Groves and Boxer, 1995). It was shown that these steady-state concentration profiles can be quantitatively described by a competition between electric field-induced drift and diffusion, thus providing a simple and predictable way of electrically creating spatial variations in the composition of a bilayer membrane.

Planar supported membranes were originally developed for studies of cell-cell recognition in the immune system, where they have proven to be highly useful (McConnell et al., 1986; Watts and McConnell, 1987). It was shown that purified major histocompatibility complex (MHC) protein incorporated into a supported membrane can replace the antigen-presenting cell in the presentation of a preprocessed antigen to a helper T-cell. However, MHC is immobile in the supported bilayer, despite the persistent fluidity of the surrounding lipid. This has also been observed for the photosynthetic reaction center, which is fully functional, yet immobilized, in the supported membrane (Salafsky et al., 1996). It is likely that this immobilization, which appears to be a general feature of transmembrane proteins in supported bilayers, results from direct interactions between the protein and the solid support (Kühner et al., 1994). Proteins tethered to the membrane by glycan-phosphatidyl inositol (GPI) linkages do not present this problem and are highly mobile (Chan et al., 1991; Fein et al., 1993). There are numerous naturally occuring GPI-linked proteins, including hydrolytic enzymes, parasite coat proteins, lymphoid antigens, small molecule receptors, as well as a variety of cell adhesion molecules (Cross, 1990; Englund, 1993). In addition, many more proteins can be genetically engineered to have a GPI linkage (Caras et al., 1987; Whitehorn et al., 1995). Incorporation of a GPI attachment signal into a gene will cause the protein to be posttranslationally modified by the cell, resulting in a GPI linkage at the signal position. This type of alteration generally does not affect the molecular recognition properties of proteins such as the ones described here (Lin et al., 1990; McHugh et al., 1995; Wettstein et al., 1991).

In this work the electric field-induced motion of GPI-tethered proteins in supported bilayers is examined. The I-E^k and B7-2 studied here have been genetically modified to replace their transmembrane domains with the GPI linkage; CD48 is naturally GPI-linked. All three proteins are mobile in supported bilayers and can easily be corralled into highly concentrated regions or spread into shallow concentration gradients through the use of electric fields and dif-

Received for publication 24 June 1996 and in final form 23 August 1996.
Address reprint requests to Dr. Jay T. Groves, Department of Chemistry, Stanford University, Stanford, CA 94305-5080. Tel.: 415-723-0386; Fax: 415-723-4817; E-mail: jtg@leland.stanford.edu.

0006-3495/96/11/2716/08 $2.00

fusion barriers. Nearly close-packed densities can be achieved while preserving the fluidity and structure of the supported membrane. Measurement of drift velocities and steady-state concentration profiles of the proteins are described and compared with those of the lipid probe. All of the field-induced concentration patterns were completely reversible. The results demonstrate that the supported bilayer provides a suitable environment for the electrical manipulation of GPI-tethered proteins.

MATERIALS AND METHODS

Pr teins

Expression systems for CD48 (Kato et al., 1992; Wong et al., 1990) and B7-2 (Azuma et al., 1993; Freeman et al., 1993; Hathcock et al., 1993) were established. Although this is not strictly necessary for CD48, it facilitates isolation of the protein in larger amounts. Mouse CD48 was amplified by polymerase chain reaction (PCR) from a mouse lymph node cDNA using the oligonucleotides 5'-AGTCATCTAGATTCTCTAAG-TATTATGTGCTTC-3' and 5'-AGTCAGAATTCGTTCTTGTCAGGT-TAACAGG-3'. The PCR product was sequenced and cloned into the polylinker of the eukaryotic expression vector, pBJINeo (Lin et al., 1990), using the restriction endonucleases *Eco*RI and *Xba*I. Similarly, the extracellular domain of B7-2 (amino acids 1–235) was PCR amplified from a mouse lymph node cDNA using oligonucleotides 5'-ACTGAGAATTC-CGGAAGCACCCACGATGG-3' and ACTGAGCGGCCGCTTGAGT-GAAATTGAGAGGTTTGG-3'. The PCR product was sequenced and cloned into a pBJINeo derivative (Whitehorn et al., 1995) that contains a modified polylinker and the human placental alkaline phosphatase (HPAP) GPI linkage signal (Fig. 1), using restriction endonucleases *Eco*RI and *Not*I. A similarly constructed GPI-linked version of I-E^k has already been described (Wettstein et al., 1991). Chinese hamster ovary (CHO) cells were transfected by electroporation at 0.23 kV/960 μF. Transfectants were selected by fluorescence-activated cell sorting for high surface expression.

GPI-linked proteins were purified from the membrane of transfected CHO cells by detergent extraction (Schild et al., 1994). Briefly, almost confluent CHO cells were washed free of medium with phosphate-buffered saline (PBS) containing a cocktail of proteinase and phosphatase inhibitors. The cells were lysed on ice in the same buffer containing 0.5% NP-40. Nuclei and cell debris were spun out, and the supernatant was loaded on an antibody affinity column. The following antibodies were used: 14.4.4, anti-I-E^k (Ozato et al., 1980), GL1. anti-mouse B7-2 (Hathcock et al., 1993), and HM48-1, anti-mouse CD48 (Kato et al., 1992). The detergent was exchanged to 1% octoglucoside (OG) on the column, and the proteins were eluted by base (pH 11.5) containing 1% OG. After elution, either the proteins were stored in neutralized elution buffer or the buffer was exchanged with 1% OG in PBS.

```
CGGTATCGAT AAGCTTGATA TCGAATTCCT GCAGCCCGGG GGATCCACTA

GTTCTAGAGC GGCCGCCTGC CTGGAGCCCT ACACCGCCTG CGACCTGCCG
                C  L  E  P  Y  T  A  C  D  L  A

CCCCCCGCCG GCACCACCGA CGCCGCGCAC CCGGGGCGGT CCGTGGTCCC
P  P  A  G  T  T  D  A  A  H  P  G  R  S  V  V  P

CGCGTTGCTT CCTCTGCTGG CCGGGACCCT GCTGCTGCTG GAGACGGCCA
A  L  L  P  L  L  A  G  T  L  L  L  L  E  T  A  T

CTGCTCCCTG AGATT
  A  F  *
```

FIGURE 1 Sequence of the polylinker and the HPAP GPI linkage signal in the modified version of pBJINeo. The sites used for cloning the extracellular domain of B7-2 are underlined, and the protein sequence of the GPI linkage signal is given in one-letter code.

Pr t liposomes

Proteoliposomes were prepared by the detergent dialysis method with preformed small unilamellar vesicles (SUVs). The SUVs were made roughly according to the Barenholz procedure (Barenholz et al., 1977). A lipid solution in chloroform was evaporated onto the walls of a round-bottomed flask, which was then evacuated overnight. Lipids were resuspended in 25 mM Tris, pH 8.0, 50 mM NaCl (TN25/50) by vortexing moderately for several minutes. The lipid concentration at this point was around 6 mg/ml. The lipid dispersion was then probe sonicated to clarity on ice under a steady flow of argon to minimize oxidation of the unsaturated lipids. The SUVs were separated from other lipid structures by ultracentrifugation for 5 h at 192,000 *g*. The supernatant contained the SUVs with typical yields of 50–75%. SUVs were frozen and stored at −80°C. Before each proteoliposome preparation, the freshly thawed SUVs were centrifuged briefly at 20,000 *g* to remove fused lipid structures. The SUVs were composed of L-α-phosphatidylcholine from egg (egg-PC) (Avanti Polar Lipids, Alabaster, AL) with 1% by mole of the fluorescent probe, *N*-(7-nitrobenz-2-oxa-1,3-diazol-4-yl)-1,2-dihexadecanoyl-*sn*-glycero-3-phosphoethanolamine, triethylammonium salt (NBD-PE) (Molecular Probes, Eugene, OR).

Solutions of the GPI-linked proteins, at concentrations around 100 nM, were mixed with SUVs, at a lipid concentration of 1 mM, in TN25/50; the total OG concentration did not exceed 0.15%. The detergent was removed by dialysis against three changes of 1 liter of TN25/50 at 4°C. After dialysis the lipid concentration was determined using the NBD-PE absorption at 465 nm and adjusted to 0.2 mg/ml.

Supported bilayers

Planar supported bilayers were produced by spontaneous fusion of proteoliposomes or SUVs with clean glass coverslips (Corning, Corning, NY). The glass surfaces were prepared by rinsing with purified water (Millipore system, 10 MW-cm), drying under a nitrogen stream, and heating at 400°C for 5 h and were used within 8 h. The bilayer was allowed to self-assemble by placing a coverslip over an 80-μl drop of vesicle suspension in a petri dish for several minutes. The dish was then carefully filled with PBS, taking care not to allow the concentrated vesicle dispersion to contact the top of the coverslip. The supported membrane was rinsed by shaking gently. The coverslip and membrane were then transferred under buffer to a two-well coverglass chamber (Nunc, Naperville, IL) for antibody staining. Nonspecific binding of the antibody was blocked by pretreatment with 10% calf serum in RPMI; any binding of proteins from the calf serum had no apparent effect on the quality or fluidity of the supported membrane. The membrane was then incubated with a 10 μg/ml solution of the appropriate antibody in the same buffer for 1 h at room temperature. The antibodies used were the same as for the purification, all directly conjugated to the fluorescent protein phycoerythrin (PE) (Pharmingen, San Diego, CA). Unbound antibody was washed away with PBS.

Two different enzyme-linked immunosorbent assay (ELISA) protocols were used to quantitate the amount of protein incorporated into the supported bilayers. The membranes were deposited on 0.5-cm round coverslips (Bellco Glass, Vineland, NJ) in a 96-well plate. In the first protocol, the bilayers were incubated with nonconjugated antibodies, as in the staining protocol. The incubation with the primary antibody was followed by a similar incubation with an appropriate alkaline phosphatase-conjugated secondary antibody: anti-mouse IgG for I-E^k, anti-hamster IgG for CD48, and anti-rat IgG for B7-2, all from Sigma (St. Louis, MO). The ELISA was developed with Sigma 104 alkaline phosphatase substrate. Values were compared to ones obtained by directly coating I-E^k to the 96-well plate. Because it cannot be assumed that directly coated protein is recognized by antibody in the same way as membrane-tethered protein, a second ELISA protocol was used for quantification of I-E^k in a comparison under identical conditions. The bilayer was redissolved in 1% OG, and the amount of I-E^k was determined with a sandwich ELISA in the presence of detergent. 14.4.4 was covalently bound to MicroBIND-HZ (Dynatech, Chantilly, VA) following the instructions of the manufacturer. The solubilized membrane was bound to 14.4.4 in comparison to known amounts of

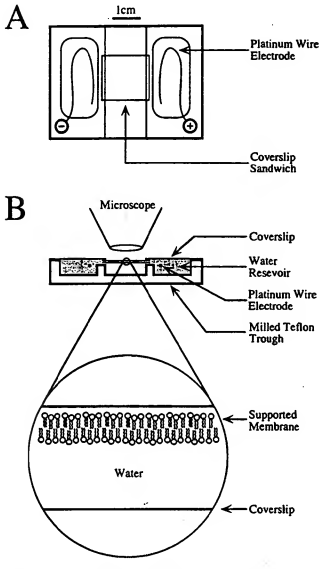

FIGURE 2 (*A*) Top view of the bilayer electrophoresis cell. The coverslip sandwich forms a bridge between the two electrode-containing wells in the Teflon trough. (*B*) Side view of the same arrangement, showing the solution-filled wells and the electrical contact achieved through the coverslip sandwich. The inset depicts a cross-section of the coverslip sandwich, illustrating the location of the supported membrane (not drawn to scale). The water layer thickness in the sandwich is in the range of 10–50 μm, which is much greater than the typical membrane thickness of 60 Å.

soluble I-E^k. The sandwich ELISA was developed with a rabbit anti-I-E^k serum (Reay and Davis, unpublished result). The two methods gave similar results: a 100 nM solution of the GPI-linked I-E^k in the detergent dialysis produced a supported bilayer with a protein density in the range of 10^{10} to 10^{11} cm^{-2}.

Membran electr ph r sis

For the electrophoretic studies, the supported membrane in PBS was diluted to 1 mM total ionic strength. Barriers to lateral diffusion were created by scratching patterns into the membrane-coated surface with a pair of tweezers. This was then assembled, under buffer, into a sandwich with another coverslip. The electrophoresis cell consisted of two 0.01" diameter platinum wire electrodes in solution-filled wells of a Teflon trough (Fig. 2).

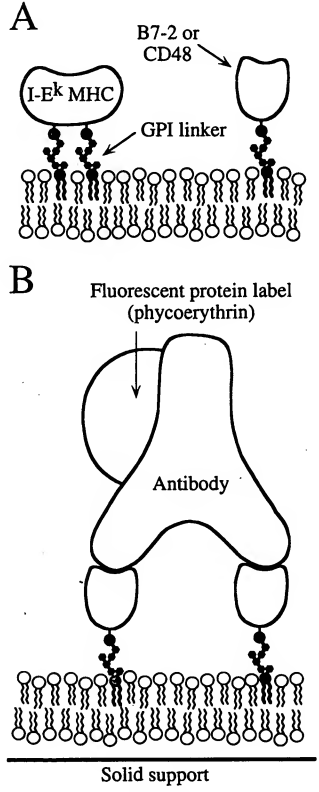

FIGURE 3 (*A*) Schematic drawings of I-E^k MHC, B7-2, and CD48 tethered to a membrane with GPI linkers. The I-E^k is a dimeric protein with two GPI linkages, whereas the monomeric B7-2 and CD48 each have one linkage. (*B*) Schematic of the fluorescently tagged antibody complexed with two GPI-tethered proteins in a supported bilayer. The exact stoichiometry of the antibody-receptor complex is not known. The sizes are roughly to scale, illustrating the extension of the protein complex away from the membrane surface.

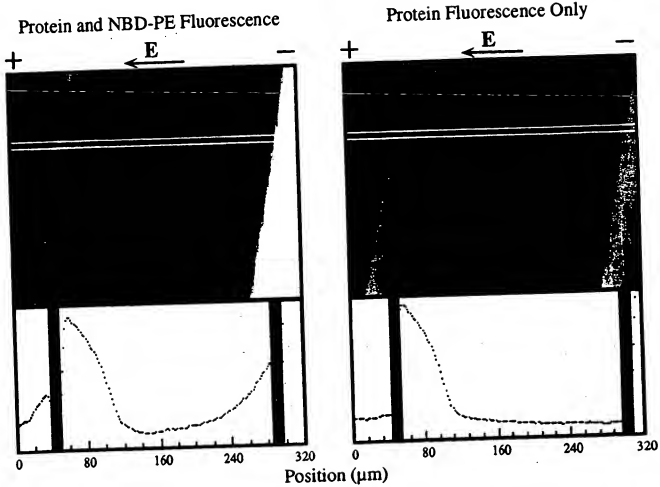

FIGURE 4 Steady-state concentration profiles of GPI-tethered B7-2 protein complex and NBD-PE lipid in a confined region of the supported membrane at a field strength of 15 V/cm. The confined region was created by scratching the membrane-coated surface with a pair of tweezers. The scratch boundaries are roughly vertical, slanting slightly to the right. The left image was taken through filters passing fluorescence from both the protein and the NBD-PE. The right image is of the same region just seconds later, viewed through filters that passed only the protein fluorescence. The fluorescence profile appearing on the anode side of the bounded region (visible in the left image only) is from the NBD-PE lipid; the protein concentration profile has built up toward the cathode. Beneath each region is a trace of the fluorescence intensity enclosed in the region between the two horizontal white lines. The vertical gray bars in these lower panels mark the positions of the scratched boundaries. It is apparent from these traces that the NBD-PE and the GPI-tethered B7-2 protein complex have different characteristic concentration profiles.

The coverslip sandwich was arranged to form a bridge between the two electrode wells. The electrical connection was achieved through the solution in the coverslip sandwich. All glass was rinsed before use to remove any residual salt deposits. Fields up to 60 V/cm were applied with a standard power supply. Currents were monitored with a Keithley picoammeter (Cleveland, OH) and were typically around 3 μA for a single 18-mm square coverslip sandwich at 15 V/cm. This corresponds to a total power dissipation of 9×10^{-5} W, which should produce a negligible amount of Joule heating. Membranes were observed in a temperature-controlled room (21°C) with an epifluorescence microscope (Zeiss, Oberkochen, Germany) through a 10× objective. Images were monitored with a low-light video camera (Cohu, San Diego, CA) and recorded with an S-VHS VCR (JVC, Elmwood Park, NJ). The camera's gamma factor ($I_{out} = I^{\gamma}$) was set at $\gamma = 1$, providing linear imaging of the fluorescence intensity.

RESULTS AND DISCUSSION

Supported membranes

Three different GPI-linked proteins have been incorporated into planar supported bilayers: CD48, B7-2, and I-E^k. CD48 is a naturally GPI-linked, monomeric lymphocyte receptor. B7-2 is a monomeric receptor on professional antigen presenting cells. A GPI-linked form of B7-2 was genetically engineered by replacing its transmembrane domain with the GPI attachment signal from HPAP. I-E^k is a heterodimeric mouse MHC class II protein with one transmembrane domain per monomer, both of which have been replaced with the GPI attachment signal. After formation of the supported bilayer, the membrane-tethered proteins were fluorescently labeled with PE-tagged antibodies (Fig. 3). The antibody does not appear to dissociate from the membrane over the time-scale of these experiments (several hours). It is expected that virtually all receptor proteins are bound to an antibody, given the vast excess of antibody used during the staining procedure. However, the exact stoichiometry of the antibody-receptor complex is not known. The relative concentrations of antibody and membrane-tethered receptors along with the observation of an apparently slow dissocia-

tion rate suggest that there is a substantial fraction of doubly bound antibody. This issue was not pursued in depth for the general study presented here. The egg-PC membrane was doped with 1% by mole of the fluorescently tagged lipid NBD-PE. Observation of the supported membranes by epi-fluorescence microscopy reveals that they are uniform to the diffraction-limited resolution of the microscope and that both the protein and the lipid are fluid with essentially no immobile fraction. Control studies with protein-free membranes indicate that there is no detectable nonspecific binding of the PE-labeled antibodies.

Under the influence of an electric field, all three membrane-tethered protein complexes drifted toward the cathode, whereas the negatively charged lipid probe NBD-PE drifted toward the anode. The major component of these membranes, egg-PC, is neutral and thus is expected to be unaffected by the field. At steady state, concentration gradients of both the NBD-PE and the GPI-tethered proteins formed in confined regions of the supported bilayer (Fig. 4). These concentration profiles were completely reversible and could be switched back and forth repeatedly by changing the direction of the electric field. When the field was removed, lateral diffusion caused the gradients to relax back to uniformity. Patterns scratched into the membrane were effective guides to lateral motion, allowing proteins to be focused into highly concentrated corrals. The triangular geometry was particularly useful for concentrating dilute components such as the I-E^k (Fig. 5). Average protein densities in the supported bilayers were estimated by ELISA to be in the range of 10^{10} to 10^{11} cm^{-2}. The degree of field-induced concentration could be ascertained by determining the area fraction of concentrated protein. For the results described here, the proteins were typically concentrated 5- to 50-fold, corresponding to nearly close-packed densities. It proved possible to create regions of supported

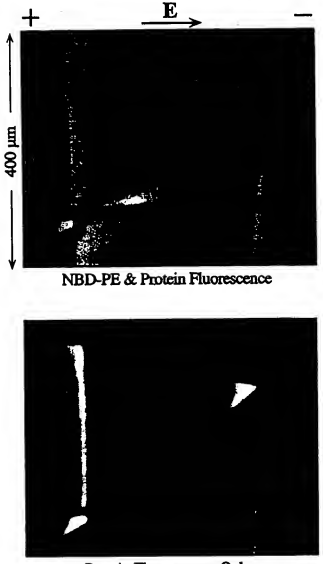

FIGURE 5 Steady-state concentration profiles of I-E^k and NBD-PE in bounded triangular regions of the supported membrane. This type of pattern is effective for generating highly concentrated domains of dilute components. The top image shows fluorescence from both the protein and the NBD-PE; the bottom shows protein fluorescence only.

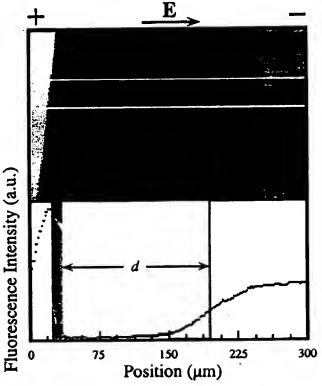

FIGURE 6 Video micrograph of the drifting image of a boundary during approach to steady state at a field strength of 15 V/cm. Below is a fluorescence intensity trace across the region between the two horizontal white lines with the scratch diffusion boundary marked with a gray bar. An image of the boundary has drifted to the right a distance *d*, as marked with a vertical line. Although the image shows significant diffusive spread, this distance can be determined accurately by locating the midpoint of the intensity profile. This image is from a CD48-containing membrane; B7-2 drift velocities were also measured in this way.

bilayer with protein concentrations several times the level at which the vesicle suspensions became unstable.

Drift velocities

The drift velocities of B7-2 and CD48 complexes were measured directly by tracking the drifting image of a boundary, as depicted in Fig. 6. Upon application of the field, all charged membrane components begin to drift with a constant average drift velocity; thus an image of the boundary will drift along with this velocity (Groves and Boxer, 1995). The image will also spread because of diffusion, but image analysis can be effectively used to locate the midpoint of this profile, allowing the image to be tracked for several minutes over more than 100 μm. Measurements taken at various times and positions in the otherwise homogeneous membrane are shown in Fig. 7. The drift velocities of both complexes are uniform and constant at 0.91 $\pm$ 0.05 μm/s for B7-2 and 0.57 $\pm$ 0.03 μm/s for CD48 at an electric field strength of 15 V/cm. It was qualitatively apparent, based on the time required to reach steady state, that I-E^k drifted substantially more slowly than either B7-2 or CD48. A plausible explanation of the reduced mobility of the I-E^k complex is that its double GPI linkage provides more drag in the viscous membrane; however, charge differences cannot be ruled out. Direct measurement of the drift velocity of the I-E^k protein complex could not be performed because it was not possible to clearly resolve the image of the boundary. The diffusive spread of a slowly drifting image can make it difficult to track.

The direction of electric field-induced drift does not necessarily indicate that the protein complex carries a net positive charge. For these experiments there generally was a bulk electroosmotic flow of solution toward the cathode on the order of 100 μm/s, as estimated by the motion of stray vesicles. Frictional coupling to this flow contributes to the drift velocity of membrane components. It has been shown that electroosmotic contributions reduce the drift velocity of negatively charged probe lipids by roughly 40% under similar experimental conditions (Groves and Boxer, 1995; Stelzle et al., 1992). Unlike the lipids, the protein complex protrudes far out of the membrane plane and is thus deeply immersed in the bulk electroosmotic flow. McLaughlin and Poo (1981) have analyzed the role of electroosmosis on the field-induced motion of molecules on the surfaces of living cells. Their analysis predicts that it is the relative difference between the zeta potentials of the protein and membrane that determines the direction of motion. If the protein is less negative than the membrane, it will move toward the cathode. Thus electroosmotic effects can dominate the motion of membrane-associated proteins.

Related experiments also provide evidence suggesting that the drift velocities of the protein complexes are sensitive to the local composition of the membrane. This sensitivity becomes apparent if the field is reversed after a concentration gradient of the protein has formed. The entire concentrated domain of protein drifts away from the boundary as a unit for a short time before substantial diffusive spreading occurs. Tracking the position of these drifting domains gave variable results. The apparent drift velocity was not constant and was always slower, by as much as 60%, than the measurements presented above for relatively uniform membranes. This discrepancy may arise from heterogeneities in surface charge density, which will, in turn, cause local variation in the electroosmotic flow. This variation can be observed directly through the trajectories of stray vesicles. Other effects such as cluster formation and percolation of oppositely drifting components may also affect the motion of protein in these concentrated domains (Scalettar and Abney, 1991).

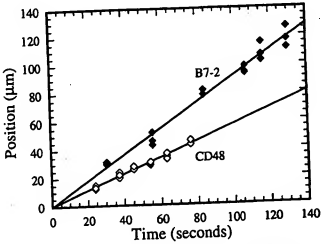

FIGURE 7 Plots of image position against drift time for the B7-2 and CD48 protein complexes. At a field strength of 15 V/cm, the drift velocity was found to be 0.91 $\pm$ 0.05 μm/s for B7-2 and 0.57 $\pm$ 0.03 μm/s for CD48.

Steady-state concentration gradients

The NBD-PE and protein built up concentration gradients in opposite directions and with different characteristic profiles (Fig. 4). Fluorescence intensity traces across these concentration profiles are plotted in Fig. 8 on a semilog scale, from which it is evident that the NBD-PE profile is single exponential, whereas the protein profile clearly shows two distinct regions, labeled I and II. Only region I appeared in the most dilute samples.

The single exponential profile observed for NBD-PE agrees with a description of this behavior as competition between field-induced drift and diffusion (Groves and Boxer, 1995). This model, which ignores all intermolecular interactions, predicts steady-state concentration profiles of the form

$$C(\mathbf{r}) = C_0 e^{\mathbf{V}\cdot\mathbf{r}/D}$$

in confined regions of the membrane; $\mathbf{V}$ is the drift velocity, D is the diffusion coefficient, and $\mathbf{r}$ is the position vector.

The drift velocity of the NBD-PE at 15 V/cm was estimated to be 0.13 ± 0.03 μm/s from this relationship by combining exponential fits of the steady-state concentration profile (giving *V/D*) with known values of the diffusion coefficient of NBD-PE in supported bilayers (4.4 ± 0.5 $\mu m/s^2$) (Stelzle et al., 1992). This value of the drift velocity is comparable to that obtained by direct measurement of a drifting boundary for Texas Red dihexadecanoyl-phosphoethanolamine (DHPE) under essentially identical conditions (Groves and Boxer, 1995). It is also interesting to note, however, that the single exponential character of the NBD-PE profile continues all the way to the scratch boundary, in contrast to the nonexponential role-off, which was observed near boundaries in profiles of the Texas Red DHPE lipid probe.

The situation with the protein is clearly more complex, as at least two well-defined regions are observed. Applying this simple model to the more dilute region I of each concentration profile, exponents (*V/D*) for B7-2 and CD48 were found to be similar, ranging from 0.09 to 0.19 μm^{-1}, whereas the I-E^k profiles typically had exponents from 0.06 to 0.10 μm^{-1}. The distinctly shallower I-E^k profile is consistent with the slower drift velocity observed for this protein. The experimental variation in these exponentials is substantially greater than that observed for the NBD-PE, likely because of the composition dependence of the drift velocity, which is much more pronounced for the protein complexes. The local drift velocities in the most dilute concentration profiles (which generally had the highest *V/D* ratios) are expected to correspond most closely to the drift velocity measurements for uniform membranes described above. Combining fit values of the exponential profiles in region I from these sampl s with drift velocity measurements such as those shown in Figs. 6 and 7 implies diffusion coefficients for the GPI-linked proteins equal to 3–6 $\mu m^2/s$, which is comparable to the lipid.

Although it seems reasonable that the model of a simple competition between field-induced drift and diffusion can be applied to region I, it is less clear that this model applies to region II, where the protein is considerably more concentrated and intermolecular interactions may be significant. It is also possible that the two regions correspond to two states of the protein complex, for example, singly and doubly bound antibodies. Further work is necessary to make connections between molecular-scale interactions and electric field-induced concentration profiles in such highly concentrated regions. However, there is evidence suggesting that these profiles can indeed be informative. Preliminary studies of streptavidin tethered to supported bilayers with biotinylated lipid reveal substantially different behavior in the highly concentrated regions. In contrast to the nearly exponential profiles observed for the GPI-tethered proteins in region II, flat profiles are observed in these regions for streptavidin. Further evidence suggests that this flat profile corresponds to the formation of two-dimensional crystalline or polycrystalline domains. More detailed studies of this system are currently under way.

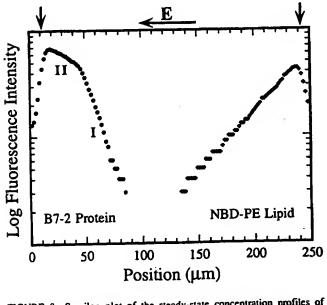

FIGURE 8 Semilog plot of the steady-state concentration profiles of NBD-PE (♦) and B7-2 protein ( ) in a bounded region of membrane. The scratch boundaries are marked with vertical arrows; the field strength was 15 V/cm as indicated. The NBD-PE concentration gradient is single exponential, whereas the protein shows two distinct, although still essentially exponential regions (labeled I and II). Only region I is observed in the most dilute samples.

CONCLUSION

The use of electric fields to manipulate GPI-tethered protein in supported bilayers has been explored. GPI-linked forms of CD48, I-E^k, and B7-2 were incorporated into supported bilayers, labeled with fluorescently tagged antibodies, and studied by epifluorescence microscopy. Under the influence of an electric field, all three protein complexes drifted toward the cathode, whereas the NBD-PE lipid probes drifted toward the anode. Steady-state concentration profiles of the NBD-PE were single exponential, in contrast to the protein profiles, which showed two distinctly different regions. Patterns scratched into the membrane were used to guide and trap both the protein and the NBD-PE lipid probe in highly concentrated corrals. Protein densities approaching close-packed were achieved. All of the field-induced concentration gradients were completely reversible and relaxed back to uniformity when the field was turned off. The GPI linkage tightly associates proteins with the supported membrane in a manner that preserves their fluidity and thus renders them susceptible to electrical manipulations. This linkage mechanism is also fairly general; the GPI attachment signal can be genetically incorporated into many different proteins.

Much of the motivation for this investigation comes from a parallel line of work in which we have integrated patterns of lateral diffusion barriers with microelectronics to construct devices capable of manipulating molecules on small length scales and in complex patterns in a supported bilayer.

One mode of operation involves the assembly of a membrane on such a microfabricated surface and subsequent electrical separation into an array of membrane patches, each with a different and precisely controlled composition. The ability to manipulate GPI-tethered proteins allows for the application of this type of device to numerous biological assays, such as screening for biological response as a function of membrane composition or protein density. It may also prove possible to manipulate proteins anchored by transmembrane helices. Electrical control of membrane-tethered proteins offers new opportunities for studies of intermolecular interactions on the surface of a membrane. Preliminary investigation of streptavidin tethered to supported bilayers with biotinylated lipid indicates that such electrical manipulations can be used to control the crystallization process.

This work was supported in part by a grant from the NSF Biophysics Program (to SGB) and by NSF grant MCB-9316256 to Professor Harden M. McConnell, who provided helpful discussions and the use of facilities in his laboratory. CW received support from an EMBO long-term fellowship. We also thank Professor Mark M. Davis for the use of facilities in his laboratory.

REFERENCES

Azuma, M., D. Ito, H. Yagita, K. Okumura, J. H. Phillips, L. L. Lanier, and C. Somoza. 1993. B70 antigen is a second ligand for CTLA-4 and CD28. *Nature.* 366:76–79.

Barenholz, Y., D. Gibbes, B. J. Litman, J. Goll, T. E. Thompson, and F. D. Carlson. 1977. A simple method for the preparation of homogeneous phospholipid vesicles. *Biochemistry.* 16:2806–2810.

Bayerl, T. M., and M. Bloom. 1990. Physical properties of single phospholipid bilayers adsorbed to micro glass beads. *Biophys. J.* 58:357–362.

Brian, A. A., and H. M. McConnell. 1984. Allogenic stimulation of cytoxic T cells by supported planar membranes. *Proc. Natl. Acad. Sci. USA.* 81:6159–6163.

Caras, I. W., G. N. Weddell, M. A. Davitz, V. Nussenzweig, and J. David W. Martin. 1987. Signal for attachment of a phospholipid membrane anchor in decay accelerating factor. *Science.* 238:1280–1283.

Chan, P.-Y., M. B. Laurence, M. L. Dustin, L. M. Ferguson, D. E. Golan, and T. A. Springer. 1991. Influence of receptor lateral mobility on adhesion strengthening between membranes containing LFA-3 and CD2. *J. Cell Biol.* 115:245–255.

Cross, G. A. M. 1990. Glycolipid anchoring of plasma membrane proteins. *Annu. Rev. Cell Biol.* 6:1–39.

Englund, P. T. 1993. The structure and biosynthesis of glycosyl phosphatidylinositol protein anchors. *Annu. Rev. Biochem.* 62:121–138.

Fein, M., J. Unkless, F. Y. S. Chuang, M. Sassaroli, R. d. Costa, H. Väänänen, and J. Eisinger. 1993. Lateral mobility of lipid analogues and GPI-anchored proteins in supported bilayers determined by fluorescent bead tracking. *J Membr. Biol.* 135:83–92.

Freeman, G. J., F. Borriello, R. J. Hodes, H. Reiser, K. S. Hathcock, G. Laszlo, A. J. McKnight, J. Kim, L. Du, D. B. Lombard, G. S. Gray, L. M. Nadler, and A. H. Sharpe. 1993. Uncovering of functional alternative CTLA-4 counter-receptor in B7-deficient mice. *Science.* 262:907–909.

Groves, J. T., and S. G. Boxer. 1995. Electric field-induced concentration gradients in planar supported bilayers. *Biophys. J.* 69:1972–1975.

Hathcock, K. S., G. Laszlo, H. B. Dickler, J. Bradshaw, P. Linsley, and R. J. Hodes. 1993. Identification of an alternative CTLA-4 ligand costimulatory for T cell activation. *Science.* 262:905–907.

Johnson, S. J., T. M. Bayerl, D. C. McDermott, G. W. Adam, A. R. Rennie, R. K. Thomas, and E. Sackmann. 1991. Structure of an adsorbed dimyristoylphosphatidylcholine bilayer measured with specular reflection of neutrons. *Biophys. J.* 59:289–294.

Kalb, E., S. Frey, and L. K. Tamm. 1992. Formation of supported planar bilayers by fusion of vesicles to supported phospholipid monolayers. *Biochim. Biophys. Acta.* 1103:307–316.

Kato, K. M., H. Okada, T. Takanashi, Y. W. Wong, A. F. Williams, K. Okumura, and H. Yagita. 1992. CD48 is a counter-receptor for mouse CD2 and is involved in T cell activation. *J. Exp. Med.* 176:1241–1249.

Kühner, M., R. Tampé, and E. Sackmann. 1994. Lipid mono- and bilayer supported on polymer films: composite polymer films on solid substrates. *Biophys. J.* 67:217–226.

Lin, A. Y., B. Devaux, A. Green, C. Sagerstrom, J. F. Elliott, and M. M. Davis. 1990. Expression of T cell antigen receptor heterodimers in a lipid-linked form. *Science.* 249:677–679.

McConnell, H. M., T. H. Watts, R. M. Weis, and A. A. Brian. 1986. Supported planar membranes in studies of cell-cell recognition in the immune system. *Biochim. Biophys. Acta.* 864:95–106.

McHugh, R. S., S. N. Ahmed, Y. C. Wang, K. W. Sell, and P. Selvaraj. 1995. Construction, purification, and functional incorporation on tumor cells of glycolipid-anchored human B7–1 (CD80). *Proc. Natl. Acad. Sci. USA.* 92:8059–8063.

McLaughlin, S., and M.-M. Poo. 1981. The role of electro-osmosis in the electric-field-induced movement of charged macromolecules on the surfaces of cells. *Biophys. J.* 34:85–93.

Ozato, K., N. Mayer, and D. H. Sachs. 1980. Hybridoma cell lines secreting monoclonal antibodies to mouse H-2 and Ia antigens. *J. Immunol.* 124:533–540.

Rädler, J., H. Strey, and E. Sackmann. 1995. Phenomenology and kinetics of lipid bilayer spreading on hydrophilic surfaces. *Langmuir.* 11:4539–4548.

Sackmann, E. 1996. Supported membranes: scientific and practical applications. *Science.* 271:43–48.

Salafsky, J., J. T. Groves, and S. G. Boxer. 1996. Architecture and function of membrane proteins in planar supported bilayers: a study with photosynthetic reaction centers. *Biochemistry.* In press.

Scalettar, B. A., and J. R. Abney. 1991. Molecular crowding and protein diffusion in biological membranes. *Comm. Mol. Cell. Biophys.* 7:79–107.

Schild, H., N. Mavaddat, C. Litzenberger, E. W. Ehrich, M. M. Davis, J. A. Bluestone, L. Matis, R. K. Draper, and Y. H. Chien. 1994. The nature of major histocompatibility complex recognition by gamma delta T cells. *Cell.* 76:29–37.

Stelzle, M., R. Miehlich, and E. Sackmann. 1992. Two-dimensional microelectrophoresis in supported lipid bilayers. *Biophys. J.* 63:1346–1354.

Watts, T. H., A. A. Brian, J. W. Kappler, P. Marrack, and H. M. McConnell. 1984. Antigen presentation by supported planar membranes containing affinity-purified I-A^d. *Proc. Natl. Acad. Sci. USA.* 81:7564–7568.

Watts, T. H., and H. M. McConnell. 1987. Biophysical aspects of antigen recognition by T cells. *Annu. Rev. Immunol.* 5:461–475.

Wettstein, D. A., J. J. Boniface, P. A. Reay, H. Schild, and M. M. Davis. 1991. Expression of a class II major histocompatibility complex (MHC) heterodimer in a lipid-linked form with enhanced peptide/soluble MHC complex formation at low pH. *J. Exp. Med.* 174:219–228.

Whitehorn, E. A., E. Tate, S. D. Yanofsky, L. Kochersperger, A. Davis, R. B. Mortensen, S. Yonkovich, K. Bell, W. J. Dower, and R. W. Barrett. 1995. A generic method for expression and use of "tagged" soluble versions of cell surface receptors. *Biotechnology.* 13:1215–1219.

Wong, Y. W., A. F. Williams, S. F. Kingsmore, and M. F. Seldin. 1990. Structure, expression, and genetic linkage of the mouse BCM1 (OX45 or Blast-1) antigen. Evidence for genetic duplication giving rise to the BCM1 region on mouse chromosome 1 and the CD2/LFA3 region on mouse chromosome 3. *J. Exp. Med.* 171:2115–2130.

Figure 1

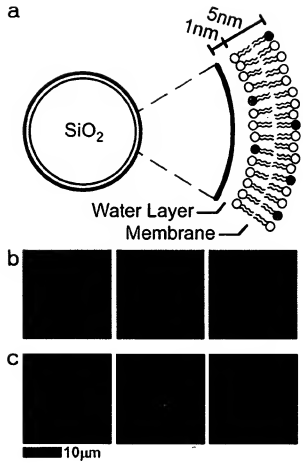

Figure 2

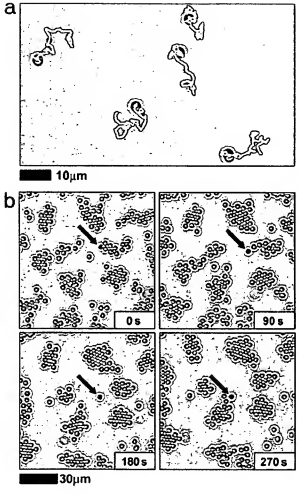

Figure 3

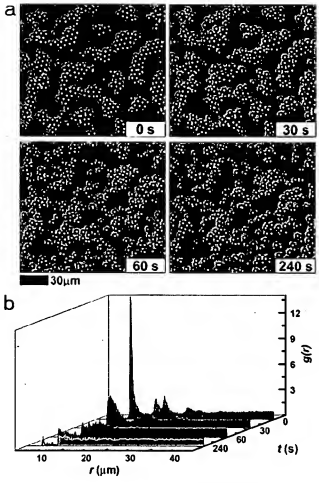

Figure 4

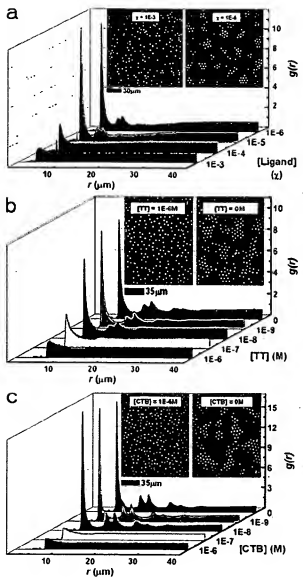

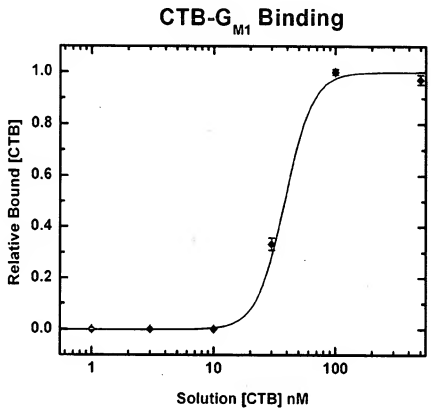

Supporting Figure 1: CTB – G_{M1} binding curve measured on planar supported membranes (89% DMOPC/ 9% DMPS/ 1% G_{M1}/ 1% Texas Red DPPE) in 18.2 MΩ-cm water. CTB binding was monitored by quantitative measurement of fluorescence from the FITC label on the CTB, and determined to have an effective dissociation constant of ~41nM All CTB used in the experiments described in this paper was FITC labeled.

Figure 5A

Figure 5B

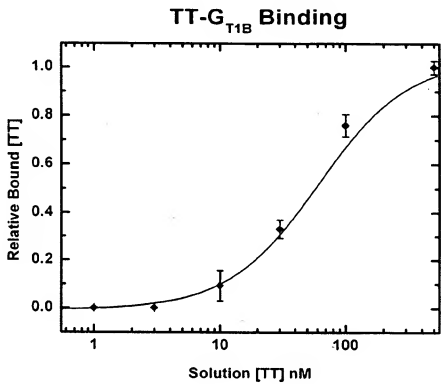

Supporting Figure 2: TT – G_{T1B} binding curve measured on planar supported membranes (89% DMOPC/ 9% DMPS/ 1% G_{T1B}/ 1% Texas Red DPPE) in 18.2 MΩ-cm water. TT binding was monitored by quantitative measurement of fluorescence from the Fluorescein label on the TT and was determined to have an effective dissociation constant of ~60nM. All TT used in the experiments described in this paper was Fluroescein labeled.

Membrane Composition	No Toxin	CTB	TT	BT	FCS	FCS + CTB
90% DMOPC, 9% DMPS, 1% Texas Red-DHPE	2.63 ± 0.07	2.52 ± 0.09	2.61 ± 0.05	2.67 ± 0.10		2.49 ± 0.05
89% DMOPC, 9% DMPS, 1% GM1, 1% Texas Red-DHPE	2.79 ± 0.10	**0.56 ± 0.12**	2.63 ± 0.05	2.84 ± 0.02	3.24 ± 0.03	**0.52 ± 0.07**
89% DMOPC, 9% DMPS, 1% GT1B, 1% Texas Red-DHPE	2.71 ± 0.09	2.47 ± 0.09	**0.46 ± 0.07**	2.71 ± 0.08		

Supporting Table 1: E_i values for several experiments. A value of Ei less than ~1 (shown in red) indicates a strongly positive signal (toxin detection).

Figure 5C

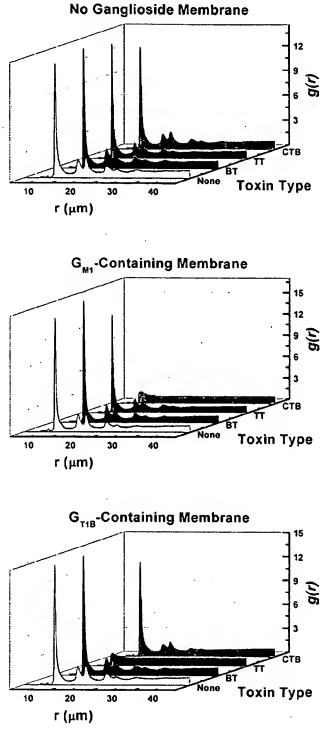

Supporting Figure 3: g(r) plots corresponding to data summarized in supporting table 1.

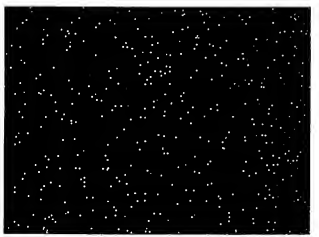

ϕ= 0.80 (-), 0.20 (+)

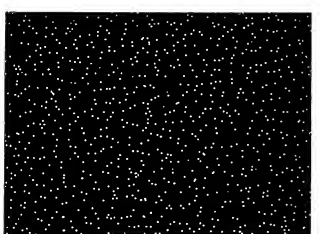

ϕ= 0.20 (-), 0.80 (+)

Figure 6

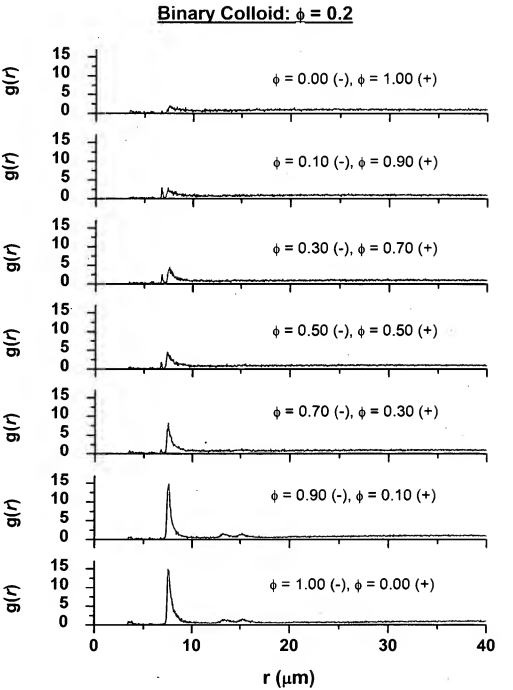

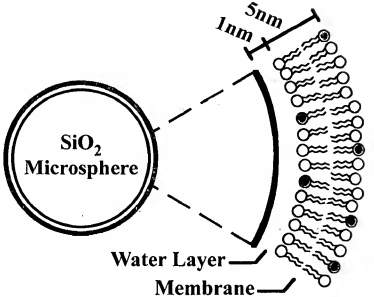

- Silica microbeads are available in sizes from ~20nm to 1000nm+.
- Can be coated with lipid bilayer membranes.

Many unique membrane system configurations can be created using this method.

Figure 7A

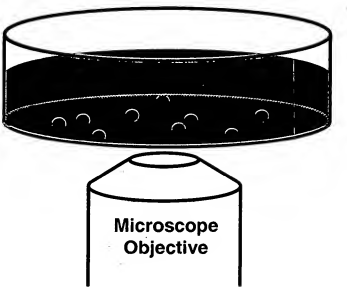

- Beads settle gravitationally to form a two-dimensional dispersion.
- Observations are made using optical microscopy.

Figure 7B